THE LATE FALL EXTRATROPICAL RESPONSE TO ENSO:

SENSITIVITY TO COUPLING AND CONVECTION

IN THE TROPICAL WEST PACIFIC

(Submitted to Journal of Climate. Revised)

June 2007

Ileana Bladé [1], Matthew Newman [2], Michael A. Alexander [3] and James D. Scott [2]

1. Departament d'Astronomia i Meteorologia, Universitat de Barcelona, Spain.

2. CIRES Climate Diagnostics Center, University of Colorado, and Physical Sciences Division/NOAA Earth System Research Laboratory (ESRL), Boulder, Colorado.

3. Physical Sciences Division/NOAA Earth System Research Laboratory (ESRL), Boulder, Colorado.

Corresponding author address: Dr. Ileana Bladé, Departament d'Astronomia i Meteorologia, Facultat de Fisica, Av. Diagonal 647, 08028 Barcelona. SPAIN. Email: ileanablade@ub.edu

Abstract

This paper provides observational and modeling evidence that the extratropical response to El Niño in late fall is modulated by anomalous forcing in the tropical west Pacific (TWP), so that a strong teleconnection is more likely when warm SST conditions prevail in the TWP. While some of these TWP SST anomalies represent noise and/or long-term variability, the results suggest that they may also be generated by differences between El Niño events, through variations in the tropical "atmospheric bridge". This bridge typically drives subsidence west of the dateline and enhanced trade winds over the far TWP, which cool the ocean. In late fall, however, some relatively weaker and/or more eastward-shifted El Niño events produce a correspondingly weakened and displaced tropical bridge, which results in no surface cooling and enhanced convection over the TWP. Because the North Pacific circulation is very sensitive to forcing from the TWP at this time of year, the final outcome is a strong extratropical El Niño teleconnection.

This hypothesis is supported by a "pacemaker" coupled simulation for the 1950-99 period, in which prescribed observed El Niño forcing in the eastern/central equatorial Pacific and an oceanic mixed-layer model elsewhere co-exist, so that the TWP is allowed to interact with the atmospheric bridge. To separate the deterministic signal driven by TWP coupling from that associated with inter-El Niño differences and from the "noise" due to intrinsic TWP convection variability (i.e., *not* induced by local SST anomalies), a second large-ensemble (100) "pacemaker" simulation of the 1997/98 El Niño event is carried out. Together, the model results suggest that coupling in the TWP can enhance the extratropical El Niño teleconnection during late fall by favoring a convective pattern that is particularly effective at forcing North Pacific circulation anomalies. Moreover, while coupling enhances the extratropical ensemble-mean response, it does not similarly increase the extratropical noise, rendering this stronger El Niño response more potentially predictable.

1. Introduction

One of the peculiarities of the extratropical response to El Niño in the Northern Hemisphere (NH) is that it does not get completely established until January, even though the abnormal warming of the tropical eastern Pacific usually peaks during late fall. This might appear to conflict with the canonical model of El Niño, in which a warm SST anomaly in the central tropical Pacific generates a widespread region of stronger-than-normal convection east of the dateline that consequently forces a wavetrain propagating across the Pacific and North America. In reality, and despite composite El Niño SST anomalies that are slightly stronger in December than January (Fig. 1c-d), it is not until January that the composite El Niño geopotential height anomaly exhibits the well-known Tropical Northern Hemisphere (TNH) teleconnection pattern (Mo and Livezey 1986) emanating out of the central equatorial Pacific (Fig. 1b). In contrast, the composite December wavetrain (Fig. 1a) has weaker amplitude and smaller scale, and displays a more zonally oriented trajectory that appears to originate in the western tropical Pacific (removing the zonal mean makes this source region even clearer). A similar distinction can be drawn using November-December and January-February averages. The tropical circulation anomalies (e.g., the pair of anticyclones straddling the Equator) are also slightly stronger in January than in December, but this difference is so minor that it seems unlikely to explain the extratropical differences. The contrast between the December and January El Niño wavetrains is not a new result (e.g., Wang and Fu 2000); yet, awareness of this large change in the ENSO teleconnection from late fall to winter is not widespread, as attested to by the large number of studies combining December and January extratropical anomalies into a December-February (DJF) winter anomaly.

The changing orientation of the El Niño wavetrain suggests that its primary source shifts

from the *western* tropical Pacific in late fall to the *central* tropical Pacific in winter. This shift (which we will show to be real) may be explained with simple Rossby waveguide arguments. Newman and Sardeshmukh (1998) showed that the sensitivity of North Pacific circulation anomalies to Rossby wave forcing over the tropical western Pacific (TWP) is much greater in late fall than in winter, whereas the opposite is true for forcing over the central Pacific (their Fig. 3). This is a result of the stronger Pacific jet in midwinter, whose associated waveguide steers Rossby waves generated in the TWP initially northeastward but then southeastward into the westerly wind duct in the eastern tropical Pacific, effectively trapping the disturbances within the tropics. In contrast, during late fall the jet is weaker but has a more pronounced zonal waveguide, so that Rossby waves emanating from the TWP can propagate across the Pacific into North America.

Variations in extratropical sensitivity to tropical forcing only matter if sufficient forcing occurs outside the equatorial central Pacific. Numerous studies have confirmed the existence of many such anomalous SST and diabatic heat sources/sinks, in the tropics and subtropics, and shown that they can impact the extratropics during both ENSO and non-ENSO situations. For example, Hamilton (1988) found that SSTs in the TWP are a major factor in determining the NH extratropical response to El Niño, with the response being most pronounced when the far western Pacific is anomalously warm (or at least not overly cold). Barsugli and Sardeshmukh (2002) suggest that tropical Pacific SST anomalies west of the dateline are very effective at exciting the PNA pattern. Extratropical responses to tropical SST anomalies in the west Pacific and Indian Oceans can be found both in models (Hoerling and Kumar 2003; Quan et al 2006; Lau et al 2006) and observations (Deser et al 2004). Several modeling studies also suggest that SST and diabatic heating anomalies over the Indian Ocean during ENSO can excite a Rossby wavetrain over the PNA region that tends to oppose the direct

response to tropical Pacific SST anomalies (Ting and Sardeshmukh 1993; Alexander et al. 2002; Annamalai et al. 2006; Barsugli et al 2006). Increased convection over the tropical and subtropical western Pacific could produce an enhanced PNA-like response (Palmer and Owen 1986) or a short-wave train (Chen 2002). Finally, adiabatic cooling over Indonesia (Branstator 1985; Ting and Hoerling 1993) and around the main central tropical Pacific heating region (DeWeaver and Nigam 2004) may also impact ENSO teleconnections. Thus, convective anomalies in the Indo-Western Pacific sector and their modulation by interactions with the ocean appear critical for a complete understanding and prediction of the extratropical response to ENSO. Moreover, their influence may vary with the annual cycle, an aspect of El Niño teleconnections that has received little attention so far.

In this paper, we provide observational and modeling evidence that the extratropical response to El Niño in late fall is modulated by anomalous TWP forcing, so that a more prominent teleconnection occurs when warm SST conditions prevail in the TWP. An important question then arises, which we will also address: could some SST variations in the TWP be driven by different "flavors" of El Niño, rather than reflect random noise and/or decadal signals? Clearly, TWP SST anomalies can be generated by local oceanic processes unrelated to ENSO, and there have been studies suggesting some long-term, even multidecadal, variability in this region (Hoerling and Kumar 2003; Deser et al 2004; Lau et al 2006; Newman 2007). On the other hand, ENSO events induce SST anomalies in the TWP through a tropical "atmospheric bridge" that involves longitudinal shifts in the regions of deep convection and in the Walker circulation (Klein et al.1999, Lau and Nath 2003). During warm events this bridge typically drives subsidence west of the dateline and enhanced trade winds over the far western Pacific that cool the ocean, further inhibiting convection. As we will show in the paper, however, some El Niño events produce a weakened tropical bridge in December, with no SST

cooling or convection in the TWP, and a strong teleconnection to the extratropics. Whether this link between the TWP and the extratropical El Niño response is coincidental (unrelated to El Niño), evidence of a causal relationship (TWP responds to the weak bridge and then drives the teleconnection), or a by-product of the perturbed tropical bridge (TWP is passive) cannot be answered solely on the basis of observations. Nor can it be diagnosed using a GCM forced with prescribed observed SSTs, for unless air/sea coupling is included, one cannot determine the role of the TWP response in *mediating* the changes to the extratropical El Niño teleconnection.

A more suitable modeling strategy to investigate cause and effect is to prescribe observed SST forcing in the tropical eastern Pacific but, elsewhere, to allow the atmosphere to interact with a mixed-layer model of ocean, following the approach originally devised by Alexander (1992a,b) and used in many studies since (e.g. Bladé 1999; Alexander et al. 2002; Lau and Nath 2003; Huang et al. 2005; Seager 2006). These so-called "pacemaker" experiments (Kinter et al. 2006) allow the El Niño response to be modulated by air/sea coupling and SST forcing in the TWP (although this forcing may be due to both the tropical atmospheric bridge and local weather noise). Furthermore, by performing parallel uncoupled simulations in which the mixed layer is replaced by climatological SSTs, we can also rule out a by-product response of the TWP to El Niño SST differences in the tropical eastern Pacific, since then the extratropical impact would tend to be the same in both coupled and uncoupled experiments. Additionally, to isolate the signal driven by coupling in the TWP from signal associated with inter-El Niño differences, we analyze a large-ensemble (100) of simulations of the 1997/98 El Niño event. This experiment also allows to separate the impacts of air-sea coupling and atmospheric noise in the TWP region.

The paper is organized as follows. After a description of the observational data, model and experiments (section 2), we examine the fall-to-winter changes in the sensitivity of the

North Pacific circulation to tropical forcing, both in nature and in the model (section 3). Having established that the model qualitatively reproduces the observed sensitivity shift, we investigate the impact of the TWP on the late fall El Niño response during the period 1950-99 (section 4). To eliminate the uncertainty introduced by the inter-event El Niño differences, we then consider the deterministic impact of coupling in a large-ensemble single-event El Niño simulation (section 5). In section 6 we discuss the seasonal changes in the relationship between TWP forcing and the extratropical circulation. Conclusions and implications of the results are presented in section 7.

2. Data, model and experiments used in this study

The observational data used in this paper are: NOAA extended SST (Smith and Reynolds 2004), NCEP/NCAR reanalysis geopotential height, SLP and surface zonal wind, and land-based rain-gauge precipitation data from the Global Historical Climate Network (GHCN; Vose et al., 1992), inverse-distance-weighted and averaged into 5ºx5º grid boxes (J. Escheid, personal communication), for the period 1950-1999 as well as for the month of December 2006 (Fig. 16). All data are converted to monthly-mean anomalies by removing the 50-year (1950-1999) mean for each month.

All experiments in this study are conducted with the GFDL R30 AGCM, which has an equivalent resolution of ~2.25º latitude by 3.75º longitude and 14 vertical sigma levels. For a description of the model and model's climate, the reader is referred to Gordon and Stern (1982), Broccoli and Manabe (1992) and Alexander and Scott (1995). In order to study the impact of air-sea coupling in the TWP on the El Niño response, we performed coupled "pacemaker" experiments, in which SSTs in the tropical eastern Pacific (15ºS-15ºN, 172ºE-South American coast) are prescribed to evolve according to observations, but air-sea

interactions are allowed elsewhere. Two sets of coupled simulations were analyzed:

- MLM–50/99 experiment: a relatively small (16 members) ensemble of globally-coupled long integrations for the period 1950-1999, which has already been used in previous studies (Alexander et al. 2002 and Lau and Nath 2003, hereafter referred to as A02 and LN03). At each oceanic grid-point outside the specified tropical eastern Pacific region, the atmosphere is coupled to a one-column entraining mixed-layer ocean model.
- TROPMLM experiment: a new "super-ensemble" (100 members) simulation of the 1997/98 El Niño event (starting in January 1996 and ending in December 1999), in which the interactive mixed-layer ocean is restricted to the tropical Indian and western Pacific oceans (between 15ºS and 15ºN). "Climatological" SSTs (see below) are specified elsewhere (outside the specified SST region).

For each set of experiments, a corresponding uncoupled control simulation (labeled CTRL–50/99 and CTRL), in which model "climatological" SSTs are specified at all oceanic grid-points (outside the specified SST region), is also performed (but will not be extensively discussed). Finally, for the single-event 4-year simulations, a NEUTRAL experiment with "climatological" SSTs prescribed over the entire oceanic domain is required to provide a basic state relative to which to compute anomalies (for the MLM–50/99 run, the anomalies are computed relative to its ensemble-mean long-term mean). The experiments consist of realizations initiated from different atmospheric conditions taken from a different simulation. The characteristics of each experiment are summarized in Table 1.

The mixed layer model has been extensively documented in Alexander et al. (2000, 2002). It simulates mixed layer temperature (or SST), salinity and depth, and includes local atmosphere-ocean fluxes, penetrating solar radiation, turbulent entrainment of water into the mixed layer and diffusion. Because of the absence of ocean currents, surface heat and salt flux

corrections are required to maintain the oceanic seasonal cycle close to observations. Small biases in SST (<1°C), however, still occur in the long-term monthly means at a few locations after the corrections are applied. Thus, for both long and short sets of integrations, a globally-coupled MLM-type experiment is performed first and its ensemble-mean long-term mean daily SSTs are used as the "climatological" SSTs in the remaining experiments. This ensures that, within each set, all experiments share the same basic state and can be compared with each other. Important physical processes such as Ekman forcing, oceanic Rossby waves and the Indonesian throughflow are missing from the coupled experiments, which may explain the weak SST anomalies simulated in the TWP (A02). We can, however, take advantage of the simplified physics in our simulations to isolate the impact of the tropical atmospheric bridge and of air/sea coupling in the TWP on the extratropical response to El Niño.

[While the original MLM–50/99 ensembles were run at GFDL, the new super-ensembles were run at ESRL. Compiler differences resulted in some differences in the mean climate and monthly variability between the GFDL MLM–50/99 runs and an identical set run on the ESRL computers. These discrepancies are notable primarily at high latitudes, but for El Niño height composites they can amount to about one contour level over the North Pacific in the figures shown herein. To be consistent with A02, all MLM–50/99 results reported here use the GFDL simulations. In all cases, the compiler differences have no qualitative impact on our results.]

The statistical significance of the differences between ensemble means or sub-ensemble means (tercile or quartile composites) is assessed via a Monte Carlo test (with replacement) for the observations and via a Student's t-test for the model results. For information on the model's El Niño signal, the reader is referred to A02 and LN03.

3. December to January changes in the extratropical sensitivity to tropical forcing:

Let us begin by showing that the spatial shift in extratropical sensitivity to tropical forcing, from the west Pacific in late fall to the central Pacific in winter, intuited from Fig. 1 and from simple Rossby waveguide arguments (as noted in the Introduction), does in fact occur. Figure 2 shows observed SST and precipitation regressed against the North Pacific Index (NPI), a measure of the strength of the Aleutian low (Trenberth and Hurrell 1994). The regressions are computed separately for December and January for the period 1950-1999, and the sign convention is chosen so that warm SST and positive precipitation anomalies are associated with a deeper Aleutian low. Clearly, the NPI is much more sensitive to TWP forcing – whether SST or precipitation – in December than in January. There is also a dramatic increase in the NPI sensitivity to SST anomalies in the central/east tropical Pacific from December to January (note that, in December, the regression is not even statistically significant).

The MLM–50/99 simulation captures this basic shift in sensitivity, albeit not as dramatically, as can be seen from corresponding calculations using model data (Fig. 3). As in the observations, the simulated SST and precipitation regressions are stronger in the TWP in December and in the central Pacific in January. The model's NPI, however, is somewhat oversensitive to central Pacific SSTs (northwest Pacific convective) forcing in December (January). This deficiency may be due to a Pacific jet in January that is weaker and farther poleward than observed (Alexander and Scott 1995), which results in modest fall-to-winter changes in the Rossby waveguide compared to nature (Newman and Sardeshmukh 1998). The model also reproduces the observed NW/SE oriented dipole of precipitation sensitivity in the TWP, with positive (negative) anomalies north (south) of Indonesia (cf. Figs. 2a and 3a), although the negative SST anomalies south of Indonesia are slightly stronger than observed.

One consequence of the less pronounced spatial/temporal shift in the extratropical sensitivity to tropical forcing, is that the simulated December El Niño height composite is more similar to the corresponding January composite than is observed (not shown, but see Fig. 13 and Fig. 12 in A02 and cf. with Fig. 1). Nevertheless, the model does capture this shift at least qualitatively; therefore, variations in the TWP (SST and/or precipitation) can still be expected to modulate the response to El Niño. Obviously, there is not necessarily a one-to-one correspondence between sensitivity to precipitation and SST (for either the model or the observations); that is, precipitation anomalies in the TWP need not arise exclusively from forcing by local SST anomalies.

4. Impact of the TWP on the extratropical response to El Niño in late fall

The discussion in the Introduction and the results of the previous section suggest that the observed El Niño extratropical response during late fall is strongly influenced by SST and convection anomalies in the TWP. To explore this possibility and guided by the December SST regression in Fig. 2, we constructed a simple index of SST in the northern tropical west Pacific region (TWP–N, to avoid confusion with TWP) by averaging (detrended[1]) monthly-mean SST anomalies over the box (3º-15ºN, 135ºE-155ºE), for the period 1950-99. We then stratified El Niño events by their December TWP–N value (Fig. 4a). The nine events chosen (also shown in Fig. 4a) are the same as those used for the composites in Fig. 1 and are those identified by Trenberth et al. (1997), to which we have added the 1997/98 event (as in A02). Based on this TWP–N index, the three events in the "HIGH" and "LOW" terciles of El Niño December months occur in 1969, 1987 and 1997 and 1965, 1972 and 1991, respectively. The years so identified are not sensitive to making the box used to define the TWP–N index either larger or smaller.

[1] The selected "HIGH" and "LOW" years (i.e., Fig. 5) are not changed if this SST index is not detrended.

Figure 5 shows difference maps of HIGH–LOW tercile composites of SST, 200 hPa height (Z_{200}), precipitation, SLP and surface zonal wind as well as the HIGH Z_{200} composite. In all these figures, anomalies should be viewed as relative to the mean El Niño pattern, not climatology. The HIGH–LOW SST pattern has warm anomalies in the TWP (by construction), particularly north of the equator, that are associated with warmer SST anomalies in the far eastern tropical Pacific and cold SST anomalies in the central tropical Pacific. The differences between the HIGH/LOW composites themselves can best be described as an absence of the cold SST "horseshoe" pattern – including the cooling in the TWP – in the HIGH composite, as well as an eastward shift in the location of the warmest SST anomalies from the central to the far eastern tropical Pacific (not shown). The corresponding HIGH–LOW precipitation anomalies are somewhat noisy but indicate enhanced convection in the TWP (also evident in the NCEP reanalysis precipitation rate, not shown). The remaining patterns are consistent with the regression results (Fig. 2), given the positive TWP precipitation and SST anomalies: the HIGH Z_{200} wavetrain response to El Niño is a stronger version of the full 9-event composite (Fig. 1) and is accompanied by a deepened Aleutian low that also extends across Alaska and the Yukon (in contrast, the corresponding LOW composite exhibits a North Pacific ridge, not shown). Moreover, the HIGH–LOW surface zonal wind pattern (Fig. 5c) suggests a weakened tropical bridge from the eastern to the western Pacific, with near-normal (enhanced) trade winds in the TWP in the HIGH (LOW) composite (not shown). The corresponding 850-hPa zonal wind and 500-hPa vertical velocity composites (not shown) confirm this weakened and eastward shifted Walker cell, with anomalous equatorial upward motion at 160ºE.

The above results suggest that the late fall differences in both the TWP and in the

extratropics between "HIGH" and "LOW" El Niño events are due to differences in the anomalous Walker cell, which in turn may be related to differences in the details of El Niño warming in the eastern tropical Pacific. That is, certain "flavors" of El Niño, characterized by a reduced and eastward shifted west-east SST gradient near the dateline, may produce a weaker bridge to the TWP. Whereas for a "typical" El Niño enhanced trade winds cool the TWP, for the "weak bridge" events the trades do not strengthen, allowing relatively warm SST conditions to persist in the TWP. These warm SSTs favor the development of convection and, because of the enhanced sensitivity of the North Pacific circulation to TWP forcing in late fall, to a stronger extratropical El Niño response.

While the observational results are consistent with the above hypothesis, they are far from conclusive. In addition to the very small sample size, we cannot distinguish between TWP SST anomalies driven by details of El Niño and its tropical bridge from those that are generated by other (oceanic) processes. Moreover, even if we had enough data to unambiguously relate TWP SST anomalies to El Niño differences, it would not necessarily mean that those TWP SSTs force the extratropical response, since the altered tropical bridge could be directly inducing the anomalous TWP convection through the same changes in surface winds and convergence that give rise to the TWP warming. That is, the changes in TWP SST would be a *by-product* of the perturbed bridge and the extratropical circulation anomalies would be directly forced by central tropical Pacific SSTs.

To address some of these issues, we perform a similar analysis on the MLM–50/99 model runs. Recall that in these runs, SST variability in the TWP can arise as a result of forcing by local weather noise or as a response to an atmospheric bridge (ENSO-induced or otherwise) and not from oceanic advection, although vertical ocean processes and air/sea feedbacks may modify both the SST and atmospheric anomalies. Additionally, each MLM–50/99

ensemble member produces different SST anomalies (outside of the specified region) for a given month, so that each El Niño event in each ensemble member can be considered an independent realization (16 x 9 samples in total). Figure 4b shows the December TWP–N index for each ensemble member during each El Niño event. Note that the intra-event variability exceeds the inter-event variability (we will return to this issue later).

Using the model's TWP–N index, we stratify our 144-member sample of December responses to produce upper and lower quartile composites (Fig. 6, comparable to the "HIGH" and "LOW" observational tercile composites in Fig. 5). The UPPER–LOWER Z_{200} pattern (Fig. 6b) indicates an enhanced El Niño wavetrain when the TWP is warmer than normal (Fig. 6f). As in the observed HIGH–LOW tercile composite, there is also warming in the far eastern Pacific, although the central Pacific is slightly warm rather than cool. Many other aspects of the observed UPPER–LOWER composite are mimicked in the simulation, including the anomalous westerly winds in the TWP (Fig. 6c) and the northeastward extension of the TWP SST anomalies into the subtropics. The precipitation pattern, however, has anomalies both in the western and central tropical Pacific and it is not clear which anomaly makes a greater contribution to the extratropical response, especially since the regression (Fig. 3) has relatively lower values east of the dateline, where the composite precipitation anomaly is largest. It is likewise unclear how much of the extratropical response is due to the TWP SST anomaly versus how much is due to event-to-event differences in tropical central Pacific convection.

We can better isolate the signal emanating from the TWP by recalling that the modeled NPI is also sensitive to negative Indonesian SST anomalies (Fig. 3). Additionally, using the NPI to form quartile composites yields UPPER–LOWER SST and precipitation patterns similar to those based on the TWP–N index (Fig. 6), but with the key differences of a

stronger TWP precipitation dipole and negative SST anomalies in Indonesia (Fig. 7). This leads us to define a second SST index measuring the strength of the SW/NE SST gradient across Indonesia, which we call the tropical western Pacific gradient (TWP–G) index, defined as the difference between the TWP–N SST anomalies and the SST anomalies averaged in a second box located southwest of New Guinea (115ºE-140ºE, 15ºS-3ºS; Fig. 8f).

Figure 8 shows UPPER–LOWER quartile composites defined using the TWP–G index; note that both regions used in the index definition are clearly visible as areas of statistically significant differences in the resulting UPPER–LOWER SST composite (Fig. 8f). The precipitation anomaly in the TWP–N region is now better defined and appears particularly sensitive in the model to the SST gradient (Fig. 8d). Consequently, the height composites indicate that, during El Niño events, a positive SW/NE SST gradient across Indonesia, with warming in the TWP–N favors convection in the TWP–N which in turn excites a well-defined Rossby wavetrain propagating across the Pacific to North America (Fig. 8b), enhancing the total El Niño response (Fig. 8a) and deepening the surface low in the North Pacific (Fig. 8e). Instead, when the TWP–G gradient is reversed, the total El Niño response in the extratropics is very weak (not shown), even though the convective forcing in the central Pacific is equally strong in the UPPER and LOWER composites. Again, many of the observed features (Fig. 5), are captured in these composites, including the high surface pressures over southeastern Asia.

As noted above, there is substantial variability of the model TWP–N SST index within each El Niño event and this is also true of the TWN–G index (Fig. 4c). There does appear to be a deterministic component to the model's SST variability in the TWP, inasmuch as some events clearly have warm (1987 and 1997) and cold (1957, 1976 and 1991) ensemble-mean TWP–N values. The sign of the ensemble-mean TWP–N index matches observations in almost all years, lending credibility to the hypothesis that these SST anomalies (and their

effect on the extratropical El Niño response) were partly driven by specific details of the SST forcing in the central/eastern tropical Pacific. Still, the large variability of the TWP indices for a single year implies that these ensemble-means are not completely determined and that the quartile composites contain not only a deterministic signal but also a random component driven by atmospheric noise. Note also that a comparison of Figs. 6 and 8 suggests that, in the model at least, the SST gradient in the TWP is less related to tropical eastern Pacific SSTs than is the TWP–N SST itself. This could be due to the incomplete sample of the mix of El Niño events that is clearly evident in Figs. 4b-c (i.e. sampling error), or to a substantial noise component driving the SST gradient.

Another source of noise that could force an extratropical response is intrinsic TWP convection variability *not* induced by local SST anomalies. Indeed, and as could be expected from Fig. 7, a much stronger extratropical signal can be found in UPPER–LOWER quartile composites based on an index of precipitation in the TWP–N region. The resulting patterns (not shown) are very similar to those in Fig. 8, but the TWP–N convective anomalies are stronger and more widespread and the height anomalies are also much more pronounced. In contrast, the SST pattern is much weaker. Both this result and the NPI-based composite (Fig. 7) suggest that North Pacific circulation is particularly sensitive to the dipole pattern of TWP precipitation, which can occur as a result of natural tropical atmospheric variability (i.e., tropical atmospheric noise) but may also be excited by SST anomalies in the TWP.

Comparison of the MLM–50/99 and CTRL–50/99 runs indicates that, in the absence of coupling, both the variability of TWP convection and the sensitivity of the North Pacific circulation to TWP convection decrease. Additionally, the ensemble-mean precipitation and Z_{200} height anomalies are significantly stronger in the MLM–50/99 experiment (not shown, but see Fig. 7a in LN03, which shows positive MLM–CTRL differences in ONDJ

precipitation in the TWP for 5 strong El Niño events, which are mostly due to differences in November and December). These results provide further evidence that coupling in the TWP enhances the extratropical December response to El Niño by promoting convection in the TWP, a region that is particularly effective at influencing the extratropical circulation.

5. Impact of the TWP on the late fall extratropical response to the 1997/98 El Niño

Drawing rigorous conclusions from the model study of the previous section is made difficult by the conflation of differences amongst El Niño events (some of which did not produce warming in the TWP) and noise in the simulations. It is unclear, for instance, to what extent the SST differences in the central/eastern Pacific in Fig. 6 are directly responsible for the differences in the extratropical response, versus how much they modify the SSTs in the TWP, which in turn modulate the response. To clarify this issue, we next describe the results of a very large ensemble of simulations of a single E1 Niño event (1997/98) concentrating on the month of December, when the event peaked and warm TWP conditions occurred both in nature and in the model (Fig. 4). Analyzing a single event allows for a much cleaner assessment of the deterministic impact of TWP coupling, which is now driven by specific details of that El Niño event, as opposed to many different events. The large ensemble also facilitates the separation of the associated extratropical signal from the noise, especially that portion of extratropical variability forced TWP precipitation noise.

Although both a globally-coupled (MLM) experiment and an experiment with the interactive mixed-layer restricted to the tropical Indian and western Pacific (TROPMLM) were performed, most of the impact of air/sea interactions on the winter extratropical response to the 1997/98 El Niño appears to be due to tropical coupling, as described in a separate study (Bladé et al., in preparation). That is, the changes in the coupled extratropical

response relative to the uncoupled response are very similar for both the MLM and the TROPMLM experiments, and the corresponding SST and precipitation anomalies in the TWP are almost indistinguishable. Thus, to further reduce the sources of noise and focus on the tropical effects, the analysis is based on the TROPMLM experiment. Moreover, because the SST anomalies in the Indian ocean are very small (see Fig 9c), our assumption throughout this paper that the impact of coupling on TWP convection is due to *local* coupling is justified.

Shown in Fig. 9 are difference maps for various ensemble-mean fields between the coupled and uncoupled experiments. The main result is that the extratropical December El Niño response is stronger in the experiment with coupling in the TWP than without coupling (Fig. 9a-b). This enhancement of the signal is tilted slightly westward with height and is relatively stronger at lower levels: the TROPMLM−CTRL differences at 200 hPa, 500 hPa, 850 hPa and at sea level, at the center of the North Pacific anomaly, are ~20%, 25%, 30% and 33%, respectively. This result replicates our earlier finding for the MLM–50/99 experiment, but the effect is now unequivocally due to the TWP SST anomalies (Fig. 9c). These include a bull's eye-like extension of the warm equatorial tongue (an artifact of the sharp boundary at 172˚E between prescribed and predicted SSTs) and weaker warm SST anomalies in the TWP and in the northern tropical Indian Ocean, as well as weak cold SST anomalies northeast of Australia. The warming in the TWP is consistent with weakened tradewinds (Fig. 9f). The observed SST anomaly for December 1997 is similar to the model's ensemble-mean response (apart from the bull's eye) and lies within the model ensemble distribution (not shown, but see Fig. 4b-c). The main coupling-induced difference in the tropical precipitation field is a patch of positive convection centered at the Equator and 160ºE (Fig. 9d), with weaker but significant negative anomalies in the eastern equatorial Indian Ocean. The results are consistent with those mentioned in the previous section for the MLM–50/99 experiment:

enhanced convection in the TWP–N results in a stronger extratropical response.

To further explore the sensitivity of the North Pacific circulation to this TWP–N convection, we stratified the TROPMLM ensemble by the TWP–N precipitation index, defined as the average precipitation within the area bounded by the 0.05 cm/day contour of TROPMLM−CTRL precipitation differences in the TWP, but only north of 3ºN (see purple line in Fig. 9d). An index defined over the entire region within this 0.05 contour is only weakly correlated with extratropical variability, possibly because the maximum on the equator straddles a node in the precipitation regression against the NPI (Fig. 3), which would imply some cancellation of its effects upon the extratropics. On the other hand, the HIGH–LOW quartile composite of Z_{200} based on the TWP–N precipitation index (Fig. 10a) exhibits a very pronounced and significant wavetrain that propagates from the TWP–N region towards the North Pacific and North America. This extratropical response is very reminiscent of that in Fig. 8, as is the corresponding SLP composite (Fig. 10b). The associated positive convective anomalies (Fig. 10c) are strong and occupy a wide band that stretches northeastward from the Equator and the dateline to the Philippines and 20ºN, with weaker negative anomalies to the south, again replicating the dipolar precipitation pattern in Fig. 8. Moreover, an "extratropical wavetrain" index defined as the difference between the (area-averaged) height anomalies in the northeast Pacific and northwest Pacific centers of action (Fig. 10a) is correlated with the TWP–N precipitation index at 0.5 (Fig. 11). Because of the large spatial extent of these positive precipitation anomalies, the results are not sensitive to the precise definition of the TWP–N precipitation box. Finally, although the corresponding SST differences are weak (Fig. 10d), they are consistent with those in Fig. 8f, i.e. a positive SW/NE SST gradient across New Guinea.

The previous results demonstrate that tropical precipitation anomalies in the TWP,

which may arise irrespective of any SST forcing (Fig. 10) but may also be generated by coupling in the TWP (Fig. 9), excite a wavetrain that interferes with the main El Niño wavetrain emanating from the central equatorial Pacific (see Fig. 13a). The result is an enhanced (damped) total El Niño response in the UPPER (LOWER) quartile composite (Fig. 10e-f). We still need to address the following questions: how does coupling change the forcing (TWP–N convection) and does coupling also change the extratropical sensitivity to that forcing? The impact of coupling on both the ensemble-mean and variability of TWP–N convection can be seen in Fig. 12, a comparison of the histograms of the TWP–N precipitation index in the TROPMLM and CTRL experiments, for December 1997 and January 1998. Because of the large sampling size, these histograms can be used to estimate the probability distribution functions (PDF) of the TWP–N index. While coupling significantly affects convection in the TWP–N region in December, its effects in January are minimal. Moreover, the coupling-induced changes in December are not linear: the TROPMLM PDF is not merely shifted towards heavier mean precipitation relative to CTRL, but has increased variance and is more strongly skewed towards positive values. In fact, fall precipitation variability in the TWP–N region increases significantly at all time scales, from daily to seasonal (not shown).

Why does coupling enhance convection in the TWP–N in late fall? The monthly-mean SST in this region is ~0.2º–0.8ºC warmer in TROPMLM than in CTRL (Fig. 9c). Although they are weak, these SST anomalies occur relative to the very warm basic state characteristic of the western Pacific "warm pool", where climatological SSTs exceed 29ºC — the threshold value for deep convection in observations (Graham and Barnett 1987) and in the model (not shown). One might then qualitatively expect the precipitation to be very sensitive to even modest positive SST departures, simply by virtue of the nonlinear increase

in evaporation that follows from the Clausius-Clapeyron relationship (a 0.1% increase in SST implies a 2% increase in saturated specific humidity). Enhanced evaporation and low-level humidity in the TWP–N indeed occur in the TROPMLM experiment (not shown), together with a weaker increase in surface air temperature (Fig. 9e). This low-level warming may reduce the surface pressure (Fig. 9b) hydrostatically (Lindzen and Nigam 1987) and lead to a strengthening of the surface circulation and moisture flux convergence (not shown). In this way, the mean warm SST anomalies that develop in the TWP in the coupled experiment could favor the development and/or intensification of TWP–N convective disturbances. The process may be helped by the presence of mean negative SST anomalies to the south, which also favor surface convergence in the TWP–N. Feedback with anomalous SST may also play some role: the correlation between the TWP–G SST and TWP–N precipitation indices is 0.37.

The coupling-induced shift in the December TWP–N precipitation PDF impacts the extratropics, as indicated by Figs. 9a-b, and as can also be seen in a scatter plot of the TWP–N index against the extratropical wavetrain index (Fig. 11). Note that there is substantial overlap of the clouds of points from the TROPMLM and CTRL experiments, and both exhibit the same correlation between the TWP–N and wavetrain indices (~0.5). This result again suggests that the tropical precipitation/extratropical response relationship itself does not depend upon coupling. To first order then, the effect of coupling is to shift the distribution of TWP–N convection towards higher values, which results in a shift of the Z_{200} distribution towards higher (negative) values and hence a stronger ensemble-mean response (see thick dot and plus marks in Fig. 11). At the same time, despite the increase in TWP–N variance, the Z_{200} variance decreases slightly (although not significantly), an outcome that could potentially arise from a saturation of the height response to increasing forcing (i.e.,

stronger positive convective anomalies). While the quadratic fit (dashed line) in Fig. 11 is suggestive of such a weakly nonlinear relationship, it cannot be distinguished from the linear fit (solid line) using an F-test, even though we have 250 samples.

The key point in the above discussion is that, while coupling in the TWP significantly enhances the *mean* extratropical El Niño response, the concurrent increase of "noise" in the forcing (TWP–N precipitation) does not appear to increase the extratropical variance. This implies that coupling increases the signal-to-noise ratio of the North Pacific 200-hPa height response (from about 1.1 to 1.3). Since potential forecast skill of monthly-mean anomalies depends upon the signal-to-noise ratio (e.g., Sardeshmukh et al. 2000), this result suggests that air-sea coupling in the TWP may make the late fall extratropical response to El Niño more potentially predictable.

6. Impact of the annual cycle on the sensitivity of the extratropical circulation to TWP forcing:

Finally, one reason we focused upon the December response to the 1997/98 El Niño is that coupling has virtually no effect on the extratropical January 1998 response (Fig. 13b-d). Thus, to fully understand how coupling in the TWP impacts the late fall response to El Niño, it may also be necessary to understand why this effect is limited to late fall. Recall that, in the model, the extratropics remain somewhat sensitive to TWP–N precipitation in January, even if this is erroneously so (cf. the regression in Fig. 3). Also, application of the quartile composite analysis to other winter months and to other years in the super-ensemble experiments reveals that, regardless of SST or coupling conditions, convection in the TWP–N region tends to generate a strong low over the North Pacific throughout the winter (November through February). This is true even for La Niña winters and for the NEUTRAL experiment. But there is one exception, and it occurs precisely during mid-winter of the El Niño year, whereupon the

sensitivity of the North Pacific circulation to anomalous convective heating in the TWP–N region seems to vanish. To illustrate this finding, Fig. 14 shows Z_{200} and precipitation UPPER−LOWER quartile composite differences, based on the TWP–N precipitation index, for December, January and February of a non-ENSO winter (1996/97) and of the Niño winter (1997/98), for the CTRL experiment. For the non-ENSO winter, convection in the TWP–N region excites a pattern of extratropical height anomalies very similar to that in Fig. 10a in all months (although in February 1997 the source region of the wavetrain is less distinct). This wavetrain is also present in December of the El Niño winter but is mostly absent in January and totally absent in February 1998. In January, one can still see a response to TWP–N heating, but it is more zonally symmetric and appears trapped in the subtropics.

This change in the "teleconnectivity" of the TWP–N region appears related to subtle ENSO-induced variations in the basic state rather than to differences in the tropical forcing, since the amplitude and extent of the TWP–N precipitation anomalies is comparable in all six cases in Fig. 14. As noted in section 3, the somewhat weaker climatological January jet could make the model's extratropics too sensitive to Rossby wave forcing over the TWP. During January and February 1998, on the other hand, the simulated El Niño-perturbed jet is stronger (not shown), so that the response to TWP forcing will be trapped in the Tropics, and the observed seasonal shift of sensitivity, from the western Pacific in late fall to the central tropical Pacific in winter, can then also occur in the model.

Additionally, in January, the impact of coupling on TWP–N convection itself is much weaker, as indicated by Fig. 12c-d and Fig. 13f (note the absence of shading). This may be due to a number of factors. First, in January, the mean state in the TWP is between 0.5 and 1ºC cooler (not shown). The coupled SST anomalies are also weaker and the SW/NE SST gradient across the TWP becomes negative (Fig. 13h). More important, the main area of

ENSO-induced convection in the central equatorial Pacific is displaced south and precipitation in the TWP–N region is now strongly suppressed (Fig. 13f). Both the presence of mean subsidence and unfavorable SST conditions may explain why, in mid-winter, coupling no longer promotes convection over the TWP–N region.

Although the simulated January and December responses to El Niño are more similar than is observed (as already mentioned), it is interesting that the model does reproduce one aspect of the observed January-to-December differences, namely a more pronounced hemispheric-wide, zonally symmetric, subtropical component in January, with elongated troughs over the southeastern coasts of Asia and North America (cf. Fig.1a-b and Fig. 13a-d). This fall-to-winter transition in the character of the mean El Niño response occurs as the negative convective anomalies spread to the TWP–N region (Fig. 13f) and is reminiscent of the changes in the teleconnectivity of the TWP–N region from December to January (Fig. 14b-d). Those negative TWP–N convective anomalies are maximized in the *LOWER* quartile El Niño composite for January 1998. Inspection of the corresponding height anomalies (not shown) reveals stronger elongated troughs over southeastern Asia and the southeastern US compared to the UPPER composite (or the ensemble-mean pattern in Fig. 13b), which account for the positive, zonally symmetric, UPPER–LOWER subtropical features in Fig. 14d. Hence, in the same TWP–N region where anomalous convection in late fall favors the development of a stronger El Niño teleconnection, suppressed convection in winter confers a more hemispheric-wide, zonally symmetric, subtropical component to the El Niño response. These results therefore suggest that the longitudinally-symmetric subtropical component of the *observed* El Niño response in mid-winter is due to the diabatic cooling (negative precipitation anomalies) in the TWP–N.

7. Summary and Concluding Remarks:

The observational and modeling results presented in this study indicate that there is a dramatic seasonal and spatial shift in the sensitivity of the North Pacific/North American circulation, from the tropical western Pacific (TWP) in late fall to the tropical central/eastern Pacific (TEP) in winter. This shift, which is consistent with the attendant changes in the basic state jet and associated Rossby wave guide (Newman and Sardeshmukh 1998), implies that the SST and/or convective anomalies in the TWP can potentially play a prominent role in forcing extratropical flow anomalies in late fall. In particular, the El Niño teleconnection at this time of year appears to be determined to a large extent by forcing in the TWP, being substantially stronger when warm conditions and convection prevail in the northern TWP.

In light of our results, we propose the following hypothesis for El Niño teleconnections, illustrated by the cartoon in Fig. 15. In winter, the tropical bridge and the interannual SST seesaw between the TWP and the TEP (Chen 2002) are usually well established for both weak and strong El Niño events. Additionally, the North Pacific circulation is more sensitive to forcing from the TEP, so the El Niño teleconnection depends mainly upon this TEP forcing. In late fall, however, some El Niño events characterized by a reduced (and/or eastward shifted) west-east SST gradient near the dateline also feature a weakened tropical bridge to the TWP (i.e., reduced subsidence and near-normal trade winds), allowing warm oceanic conditions in the TWP that are conducive to the development of local convection (in contrast to the cold SSTs/suppressed convection that occur when the bridge is strong). Because of the enhanced sensitivity of the North Pacific circulation to forcing from the TWP in late fall, the extratropical El Niño response will be strong. The most recent 2006/07 El Niño event, which decayed rapidly in January but was strong in December, appears to agree with this picture, with warm SST and convective anomalies in the TWP and a

pronounced extratropical wavetrain response in late fall (Fig. 16).

Of course, the deterministic picture of Fig. 15 is clouded by any other source of TWP SST variability. In our coupled "pacemaker" experiments, random SST variability driven by (and coupled to) atmospheric noise clearly had an influence on whether or not the TWP was warm during a particular realization of a given El Niño event. Moreover, in nature, SST variability can also result from oceanic processes that may not be deterministically influenced by event-to-event El Niño differences, or from long-term variability unrelated to El Niño. Still, many aspects of the observed composites were reproduced in our "pacemaker" experiments (in which SST variability in the TWP can only occur in response to atmospheric forcing), including how the tropical bridge responded to different El Niño events. Furthermore, a very large ensemble simulation of the single 1997/98 El Niño event allowed for unambiguous identification of the deterministic impact of coupling in the TWP on the extratropical El Niño response. This experiment revealed a clear enhancement of the coupled El Niño teleconnection during late fall as a result of warming in the TWP that in turn favored the development of convection in the northern TWP, a forcing region to which the extratropics is particularly sensitive. Coupling also appeared to increase the El Niño signal-to-noise ratio (i.e., the potential predictability) in the extratropics for this event, despite an increase in the spread (noise) of the tropical forcing. Taken together, our model results support the view that the late fall SST differences in the TWP from event to event – and their impact on the nature and predictability of the extratropical El Niño response – are partly deterministic and driven by details of the El Niño SST anomalies in the TEP, via changes in the tropical atmospheric bridge.

Because of a relatively weak simulated jet, the teleconnectivity between TWP convection and North Pacific circulation is generally present throughout the winter in the

model. An exception occurs when a strong El Niño event intensifies the jet, allowing the model to mimic the observed pronounced decrease in North Pacific sensitivity to TWP forcing from December to January. Yet, forcing from the TWP continues to impact the El Niño response, though in a different region: the suppressed convection that develops over the TWP at this time appears to force the hemispheric-wide, longitudinally symmetric, *subtropical* component of the winter El Niño teleconnection. This result suggests that the TWP region may account for a large fraction of the extratropical response in experiments with prescribed SST forcing in a broad "tropical Indo-Western Pacific" (IWP) region (at least in the GFDL model). For instance, the DJF response to continuous warming in the IWP region during the 1998-2002 period in Lau et al.'s (2006) experiment exhibits zonally elongated ridges across the subtropics that are very reminiscent of the simulated anomalies produced by TWP convection in January (Fig. 14d).

Our results serve to reiterate the point (perhaps often overlooked, although undoubtedly familiar to seasonal forecasters/analysts) that the "canonical" view of the El Niño teleconnection, a TNH-like wavetrain emanating from the central/eastern equatorial Pacific (and modified by interactions with the basic state and transient eddies), is more appropriate in mid-winter than in late fall (e.g., Wang and Fu 2000). Diagnostic studies using DJF seasonal averages may therefore obscure some important aspects of climate anomalies associated with El Niño.

While our focus has been on El Niño, the results are also relevant for La Niña and non-ENSO situations characterized by convective forcing in the TWP, such as occur, for instance, during the passage of MJO disturbances. For example, the presence of warm SST anomalies and convection in the TWP in December during the La Niña 2005/06 event may explain why the circulation responded with a roaring North Pacific jet more characteristic

of El Niño conditions, even though the SST and convective anomalies in the TEP were typical of a La Niña (K. Weickmann, personal communication). Several previous studies have demonstrated a relationship between SST and/or convective forcing in the TWP and atmospheric circulation anomalies over the North Pacific/North America in winter, both during El Niño (Hamilton 1988, Chen 2002) and in general (Simmons et al. 1983, Palmer and Owen 1986, Quan et al 2006). Yet, our results suggest that they may have mixed together late fall and winter effects. Additionally, Quan et al. (2006)'s identification of the (subtropical) TWP as an important *non-ENSO* source of skill over the U.S. during late fall may have been premature, for some of this skill could have been due to ENSO effects in the TWP region.

Another possible implication of our results concerns the PDO (Pacific Decadal Oscillation), the leading pattern of North Pacific SST variability (Mantua et al. 1997). The observed HIGH–LOW December El Niño composite displays a strong negative SST anomaly in the North Pacific (Fig. 5) that resembles the PDO. A weak cold North Pacific SST anomaly is also evident in the MLM–50/99 composites, and a strong PDO-like signal also appears in the MLM 150-member simulation in December 1997 (not shown), where it has virtually no effect upon the atmosphere, as was noted above. This raises the possibility that, during late fall, variations in TWP SSTs may help force variations in the PDO, in contrast to the remainder of the year where TEP SSTs typically lead the PDO by a few months (Newman et al. 2003). Moreover, to the extent that positive TWP SSTs and a high PDO phase may occur together during relatively weak El Niño events, this relationship may help explain the fall minimum in the ENSO-PDO correlation (Newman et al. 2003) as well as suggest some tropical origins for the varying extratropical ENSO patterns during combinations of high and low ENSO and PDO phases (e.g., Gershunov and Barnett 1998).

Finally, our results do not appear to depend upon the recent warming trend in the TWP, since the trend was still weak during the 1950-99 period and the observational composite is unchanged if the data is first detrended. Even in the presence of a long-term trend, event-to-event differences in the tropical bridge might result in corresponding differences in ENSO-induced TWP anomalies. Our results may have implications for how the climate will be affected if the TWP region continues to warm and suggest, in particular, that the effects may be different during late fall than in winter.

Acknowledgments:

We are very grateful to John Young and Brian Mapes whose comments, suggestions and enthusiasm provided a big motivation for this study and greatly improved the manuscript. Gil Compo and Klaus Weickmann also made insightful comments. The constructive suggestions by two anonymous reviewers lead to substantial clarification of some of the issues addressed in this article. Thanks are also due to Jon Escheid for supplying the gridded GHCN precipitation data and to Jennifer M. Adams for help with GrADs. IB is a researcher supported by the Ramón y Cajal Program, funded by the Spanish MCYT.

References

Alexander, M. A., 1992a: Midlatitude atmosphere-ocean interaction during El Niño. Part I: the North Pacific Ocean. *J. Climate*, 5, 944-958.

Alexander, M. A., 1992b: Midlatitude atmosphere-ocean interaction during El Niño. Part II: the North hemisphere atmosphere. *J. Climate*, **5**, 959-972.

Alexander, M. A., and J. D. Scott, 1995: Atlas of climatology and variability in the GFDL R30S14 GCM. CIRES, Univ. of Colorado, 121 pp. [Available from the authors at CDC/NOAA, R/CDC1, 325 Broadway, Boulder, CO. 80305-3328].

Alexander, M. A., J. D. Scott, and C. Deser, 2000: Processes that influence sea surface temperature and ocean mixed layer depth variability in a coupled model. *J. Geophys. Res*., **105**, 16,823-16,842.

Alexander, M. A., I. Bladé, M. Newman, J. R. Lanzante, N.-C. Lau, and J. D. Scott, 2002: The atmospheric bridge: the influence of ENSO teleconnections on air-sea interaction over the global oceans. *J. Climate*, 15, 2205-2231

Alexander, M. A. and J. D. Scott, 2002: The influence of ENSO on air-sea interaction in the Atlantic. *Geophys. Res. Lett*., **29(14)**, 10.1029/2001GL014347.

Annamalai, H., H. Okajima, and M. Watanabe, 2006: Possible Impact of the Indian Ocean SST on the Northern Hemisphere Circulation during El Nino. *J. Climate*, **20**, 3164-3189.

Barsugli, J. J., and P. D. Sardeshmukh, 2002: Global atmospheric sensitivity to tropical SST anomalies throughout the Indo-Pacific Basin. *J. Climate,* **15,** 3427-3442.

Bladé, I., 1999: The influence of midlatitude ocean-atmosphere coupling on the low-frequency variability of a GCM. Part II: Interannual variability induced by tropical SST

forcing. *J. Climate*, **12**, 21-45.

Branstator, G., 1985: Analysis of General Circulation Model Sea-Surface Temperature Anomaly Simulations Using a Linear Model. Part I: Forced Solutions. *J. Atmos. Sci*., **42**, 2225-2241.

Broccoli, A. J., and S. Manabe, 1992: The effects of orography on midlatitude Northern Hemisphere dry climates. *J. Climate*, **5**, 1181-1201.

Chen, T.-C., 2002: A North Pacific short-wave train during the extreme phases of ENSO. *J. Climate*, **15**, 2359-2376.

Deser, C., Adam S. Phillips, and James W. Hurrell, 2004: Pacific Interdecadal Climate Variability: Linkages between the Tropics and North Pacific during boreal winter since 1900. *J. Climate,* **17**, 3109-3124.

DeWeaver, E., and S. Nigam, 2004: On the forcing of ENSO teleconnections by anomalous heating and cooling. *J. Climate*, **17**, 3225-3235.

Gershunov A., and T. P. Barnett, 1998: Interdecadal modulation of ENSO teleconnections. *Bull. Amer. Meteor. Soc.*, **79**, 2715–2725.

Graham, N. E., and T. P. Barnett, 1987: Sea surface temperature, surface wind divergence and convection over tropical oceans. *Science*, **238**, 657-659

Gordon, C. T., and W. F. Stern, 1982: A description of the GFDL global spectral model. *Mon. Wea. Rev*., **110**, 625-644.

Hamilton, K., 1988: A detailed examination of the extratropical response to tropical El Niño/Southern Oscillation events. *J. Climatol.*, **8**, 67-86.

Hoerling, M. P., and A. Kumar, 2003: The perfect ocean for drought. *Science*, **299**, 691-

694.

Huang, H.-P., R. Seager and Y. Kushnir, 2005: The 1976/77 transition in precipitation over the Americas and the influence of tropical SST. *Clim. Dyn*., **24**, 721-740.

Kinter, J., C. K. Folland and B. P. Kirtman, 2006: Workshop on Climate of the 20th Century and Seasonal to Interannual Climate Prediction. *CLIVAR Exchanges,* **11***,* 30-31.

Klein, S. A., B. J. Soden, and N-C. Lau, 1999: Remote sea surface temperature variations during ENSO: Evidence for a tropical atmospheric bridge. *J Climate,* **12**, 917-932.

Lau, N-C., and M. J. Nath, 2003: Atmosphere-ocean variations in the Indo-Pacific sector during ENSO episodes. *J. Climate*, **16**, 3-20.

Lau, N.-C., A. Leetmaa and M. J. Nath, 2006: Attribution of atmospheric variations in the 1997-2003 period to SST anomalies in the Pacific and Indian Ocean basins. *J. Climate*, **19**, 3607-3628.

Lindzen, R.S., and S. Nigam, 1987: On the role of sea surface temperature gradients in forcing low-level winds and convergence in the tropics. *J. Atmos. Sci*., **44**, 2418-2436.

Mantua N. J., S. R. Hare, Y. Zhang, J. M. Wallace, and R. Francis, 1997: A Pacific interdecadal climate oscillation with impacts on salmon production. *Bull. Amer. Meteor. Soc.*, **78**, 1069–1079.

Mo, K. C., and R. E. Livezey, 1986: Tropical-extratropical geopotential height teleconnections during the Northern Hemisphere winter. *Mon. Wea. Rev*., **114**, 2488-2515.

Newman, M., and P. D. Sardeshmukh, 1998: The impact of the annual cycle on the North Pacific/North American response to remote low frequency forcing. *J. Atmos. Sci*., **55**, 1336-1353.

Newman M., G. P. Compo, and M. A. Alexander, 2003: ENSO-forced variability of the Pacific decadal oscillation. *J. Climate*, **16**, 3853–3857.

Newman, M., 2007: Interannual to decadal predictability of tropical and North Pacific sea surface temperatures. *J. Climate*, **20**, 2333-2356.

Palmer, T. N. and J. A. Owen, 1986: A possible relationship between some "severe" winters in North America and enhanced convective activity over the Tropical west Pacific. *Mon. Wea. Rev.*, **114**, 648-651.

Quan, X., M. Hoerling, J. Whitaker, G. Bates, and T. Xu, 2006: Diagnosing Sources of U.S. Seasonal Forecast Skill. *J. Climate*, **19**, 3279-3293.

Sardeshmukh, P. D., G. P. Compo, and C. Penland, 2000: Changes of probability associated with El Niño. *J. Climate*, **13**, 4268-4286.

Simmons, A. J., J. M. Wallace, and G. W. Branstator, 1983: Barotropic Wave Propagation and Instability, and Atmospheric Teleconnection Patterns. *J. Atmos. Sci.*, **40**, 1363-1392.

Seager, R., 2006: The Turn of the Century drought across North America: global context, dynamics and past analogues. *Journal of Climate* forthcoming. [online].

Seager, R., N. Harnik, Y. Kushnir, W. Robinson and J. Miller(Velez), 2003: Mechanisms of hemispherically symmetric climate variability. *Journal of Climate*, 16(18): 2960-2978.

Smith, T.M., and R.W. Reynolds, 2004: Improved Extended Reconstruction of SST (1854-1997). *Journal of Climate*, **17**, 2466-2477.

Ting, M. F. and P. D. Sardeshmukh, 1993: Factors Determining the Extratropical Response to Equatorial Diabatic Heating Anomalies. *Journal of the Atmospheric Sciences*, **50**, 907-918.

Ting, M., and M. P. Hoerling, 1993: Dynamics of stationary wave anomalies during the 1986/87 El Niño, *Climate Dynamics*, **9**, 147-164.

Trenberth, K.E. and J.W. Hurrell, 1994: Decadal Atmosphere-Ocean Variations in the Pacific. *Climate Dynamics*, **9**, 303-319.

Trenberth, K. E., 1997: The definition of El Niño. *Bull. Amer. Met. Soc.*, **78**, 2771-2777.

Vose, R. S., R. L. Schmoyer, P. M. Steurer, T. C. Peterson, R. Heim, T. R. Karl, and J. K. Eischeid, 1992: The Global Historical Climatology Network: Long-term monthly temperature, precipitation, sea-level pressure, and station pressure data. Rep. ORNL/CDIAC-53, Carbon Dioxide Inf. Anal. Cent., Oak Ridge Natl. Lab., Oak Ridge, TN, 25pp.

Wang, H., and R. Fu, 2000: Winter monthly mean atmospheric anomalies over the North Pacific and North America associated with El Niño SSTs. *J. Climate*, **13**, 3435-3447.

Figure Captions

FIGURE 1. Observed December and January composite anomalies of 200-hPa geopotential height and SST for 9 moderate to strong El Niño events that occurred during the period 1950-1999 (1957/58, 1965/66, 1969/70, 1972/73, 1976/77, 1982/83, 1987/88, 1991/92 and 1997/98). The anomalies are computed relative to the 1950-1999 climatology. Contour interval is 15 m for geopotential height and 0.4 K for SST. Negative contours are lightly shaded. SST anomalies greater than 2 K are shaded in dark grey. The thin line is the zero contour.

FIGURE 2. Top: Observed regressions of December (left) and January (right) monthly precipitation against the North Pacific index (Trenberth and Hurrell 1994), for the period 1950-99. Contour interval is 0.005 cm/day. Red/yellow (blue) shadings indicate positive (negative) values. The NP index is a measure of the strength of the Aleutian low (area-weighted sea level pressure over the region 30oN-65oN, 160oE-140oW), with a standard deviation of 3.5 hPa in December and 4.4 hPa in January, and its sign has been reversed. Bottom: Same but for SST; contour interval is 0.01 K. The datasets employed are gridded GHCN precipitation (land-based rain-gauge station data, averaged into 5ºx5º grid boxes by using an inverse-distance weighting method) and Reynolds SST (2003). The purple line indicates the regions in which the corresponding correlation is 95% statistically significant, assuming one degree of freedom per year (r=+/- 0.27)

FIGURE 3. Same as Fig. 2 but for the MLM-50/99 experiment (every model realization is considered an independent realization, i.e. the sampling size is 800). The model's NPI standard deviation is 4.1 hPa in December and 4.6 hPa in January. Contour interval as in Fig. 2. The purple line indicates the regions in which the corresponding correlation is 99%

statistically significant, assuming one degree of freedom per year (r=+/- 0.09).

FIGURE 4. Top panel: observed December TWP–N (Tropical Northwest Pacific) SST Index for the period 1950-99. The index is defined as the detrended standardized SST averaged over the region (3˚-15˚N, 135˚E-155˚E). The El Niño years are indicated with black bars. The three "LOW" and "HIGH" years, as defined by this SST index are indicated by triangles and inverted triangles, respectively. See Figs 5c or 6c for the location of the TWP–N box. Middle panel: Simulated December TWP–N SST index for the 9 El Niño years and for each realization in the MLM-50/99 experiment. The circles denote individual realizations, the black dots denote the ensemble average for each El Niño event. The dashed lines denote the 25% and 75% percentiles and indicate which realizations enter into the UPPER and LOWER quartile composites in Fig. 5. Bottom panel: Same but for the SST gradient index in the Tropical western Pacific (TWP–G). This index is defined as the normalized NW/SE SST gradient across New Guinea, specifically SST averaged over the TWP–N box minus SST averaged over the box (15˚S-3˚S, 115˚E-140˚E).) See Fig. 8c for the location of the boxes.

FIGURE 5. Observed El Niño December anomalies stratified according to the December TWP–N SST index shown in Fig. 4a, so as to produce "HIGH" and "LOW" tercile composites. Upper tercile years: are 1969, 1987 and 1997; lower tercile years are 1965, 1972 and 1991 (cf. Fig. 4a). The area used to define the TWP–N index is indicated by a box in panel f.

a) "High" composites of 200-hPa geopotential height (Z-200). Remaining panels show the corresponding "HIGH–LOW" composite differences of b) Z-200, c) tropical surface zonal

wind, d) tropical precipitation, e) SLP and f) SST. Contour/shading interval is 20 m for height, 0.067 cm/day (20 cm/month), 0.25 K for SST, 0.5 ms-1 for winds and 1 mb for SLP. Red (blue) shadings indicate positive (negative) values. The zero contour is omitted and shading starts at the lowest contour. The dotted (solid) purple line indicates statistical significance of the "HIGH-LOW" composite differences at the a posteriori (two-sided) 80% and 90% confidence levels. Note that wherever the sign of the difference is expected a priori (i.e. enhanced TWP–N convection, deeper North Pacific low, negative North Pacific heights), the significance levels are actually 90% and 95%.

FIGURE 6. Similar to Fig. 5, but for the MLM-50/99 experiment. Simulated El Niño December anomalies stratified according to the December TWP–N SST index shown in Fig. 4b, so as to produce UPPER and LOWER quartile composites (each containing 36 samples). The area used to define the TWP–N index is indicated by a box in panel f. Contour/shading interval is 20 m for height, 0.067 cm/day (20 cm/month) for precipitation, 0.15 K for SST, 0.5 ms-1 for winds and 1 mb for SLP. The zero contour is omitted and shading starts at the lowest contour. The dotted (solid) purple line indicates statistical significance of the "UPPER–LOWER" composite differences at the a posteriori (two-sided) 95% and 99% confidence levels. Note that wherever the sign of the difference is expected a priori (i.e. enhanced TWP–N convection, deeper North Pacific low, negative North Pacific heights), the significance levels are actually 97.5% and 99.5%. The absolute anomalies in panel (a) are computed relative to the ensemble-mean 50-year climatological mean.

FIGURE 7. As in the left panels of Fig. 6, but the quartile composites are based on the North Pacific index (NPI). The sign convention is such that the UPPER quartile composite

corresponds to an enhanced Aleutian low (strongly negative NPI). Contours and shading as in Fig. 6.

FIGURE 8. As in Fig. 6 but the quartile composites are based on the SST gradient index in the Tropical western Pacific, TWP–G. The areas used to define the TWP–G index are indicated by boxes in panel f. Contours and shading as in Fig. 6.

FIGURE 9. December 1997 TROPMLM – CTRL anomaly differences in a) 200-hPa height, b) SLP, c) SST, d) precipitation, e) surface air temperature, and f) surface zonal wind. Contour interval is 10 m, 0.4 mb, 0.2 K, 0.1 cm day-1, 0.2 K, and 0.3 ms-1. The zero contour is omitted. The two grades of shading denotes statistical significance of the differences at the a posteriori (two-sided) 95% and 99% confidence levels. The purple line in panel (d) indicates the averaging region used to construct the TWP–N precipitation index, and is defined by the 0.05 cm day-1 precipitation contour, north of 3ºN.

FIGURE 10. UPPER–LOWER quartile composite differences, based on the TWP–N precipitation index (see purple line in Fig. 9d), for a) 200-hPa height, b) sea level pressure, c) precipitation and d) SST in December 1997 in the TROPMLM experiment. Contour/shading interval is 20 m, 1 mb, 0.0667 cmday-1 and 0.1 K respectively. Red (blue) shadings indicate positive (negative) values. The zero contour is omitted and shading starts at the lowest contour. The dotted (solid) purple lines indicates statistical significance (95% and 99% two-sided confidence levels). The sample size in each upper/lower composite is 25. Also shown in the bottom panels are the UPPER and LOWER quartile composites of 200-hPa height (same contour interval as in panel a).

FIGURE 11. Scatter plot between the December 1997 TWP–N precipitation index and the

200-hPa North Pacific wavetrain index in experiments CTRL and TROPMLM. The precipitation index is defined as the total precipitation averaged within the purple line in Fig 9d. The 200-hPa North Pacific wavetrain index is defined as the difference between the 200-hPa anomalies averaged over the northeastern Pacific and western Pacific centers of action in Fig. 10a (areas within the -60 m contour). The number in the lower left corner indicates the correlation coefficient obtained pooling all data together. The correlation for each individual experiment is indicated in the legend box. The solid (dashed) line represents a linear (quadratic) fit to the data. The thick dot and cross represent the ensemble-mean mean CTRL and TROPMLM values respectively.

FIGURE 12. Normalized histogram (bars) and probability density function (lines), estimated with a Gaussian Kernel, of monthly-mean December 1997 (top) and January 1998 (bottom) total precipitation (in cm day-1) averaged over the TWP–N precipitation region, in the CTRL (left) and TROPMLM (right) experiments.

FIGURE 13. The December and January ensemble-mean response to El 1997/98 Niño event in the uncoupled (CTRL) and tropically-coupled (TROPMLM) experiments. Top panels: December and January Z-200 anomalies in the CTRL experiment. Below: same but for the TROPMLM experiment. Below: same but for the precipitation anomalies. Bottom panels: same but for the SST anomalies. Anomalies are computed relative to the ensemble-mean 4-year mean in the NEUTRAL experiment. The shading in the top three rows indicates statistical significance of the TROPMLM–CTRL differences at the 95% and 99% two-sided confidence levels. Contour level is 20 m, 0.2 cm/day and 0.2 K, respectively. Note that the SST anomalies in the tropical eastern Pacific, east of 172˚E, are prescribed in both the TROPMLM and CTRL experiments.

FIGURE 14. CTRL experiment. UPPER–LOWER quartile composite differences of tropical precipitation (orange and green shading) and NH extratropical 200-hPa height (red and blue shading) in December, January and February, for the non-ENSO 1996/97 winter (left panel) and for the El Niño 1997/98 winter (right panel), based on the TWP–N precipitation index (see Fig. 9d). The dashed and solid purple lines indicate statistically significant differences (95% and 99% levels). Contour interval is 0.0667 cmday-1 and 20 m. The sample size in each upper/lower composite is 38.

FIGURE 15. Schematic of proposed hypothesis for the El Niño teleconnections. In January the tropical bridge from the TEP to the TWP is generally well established for both weak and strong El Niño events, which creates cold conditions in the TWP. Additionally, the North Pacific circulation is more sensitive to forcing from the TEP, so the El Niño teleconnection is modulated by variations in this TEP forcing. In December, however, some events are characterized by a weakened tropical bridge and warm (or not cold) conditions in the TWP, which supports the development of local convection. Because of the enhanced sensitivity of the North Pacific circulation to forcing from the TWP in late fall, the extratropical El Niño response will be much stronger

FIGURE 16. Z-200, precipitation and SST December anomalies for the 2006/07 El Niño event. Contour interval is 25 m, 0.3 cm/day and 0.1 K.

Observed El Niño composites

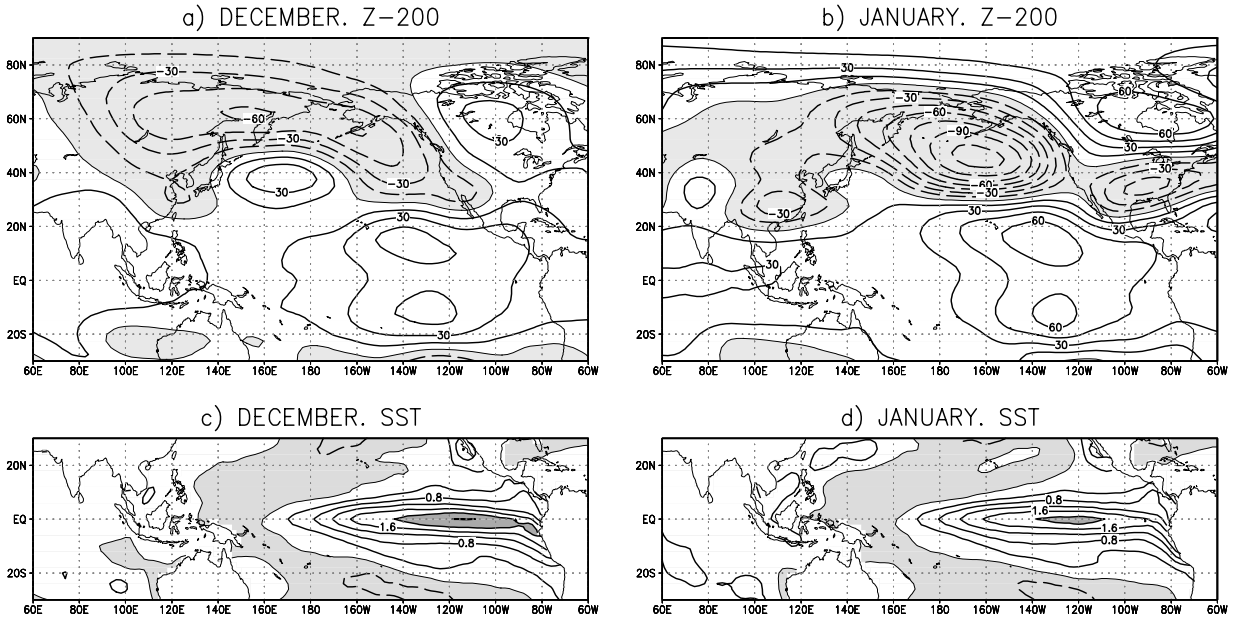

Fig. 1. Observed December and January composite anomalies of 200-hPa geopotential height and SST for 9 moderate to strong El Niño events that occurred during the period 1950-1999 (1957/58, 1965/66, 1969/70, 1972/73, 1976/77, 1982/83, 1987/88, 1991/92 and 1997/98). The anomalies are computed relative to the 1950-1999 climatology. Contour interval is 15 m for geopotential height and 0.4 K for SST. Negative contours are lightly shaded. SST anomalies greater than 2 K are shaded in dark grey. The thin line is the zero contour.

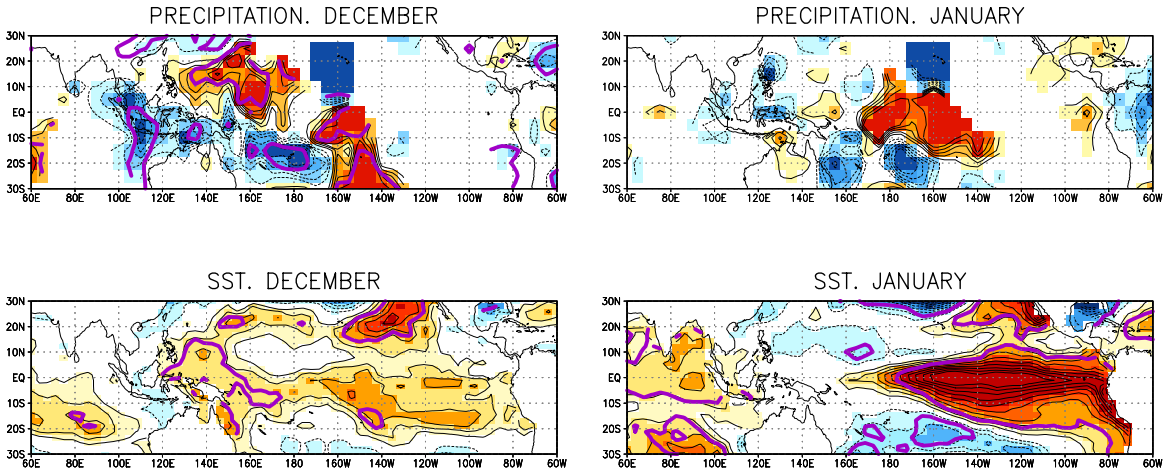

FIG. 2. Top: Observed regressions of December (left) and January (right) monthly precipitation against the North Pacific index (Trenberth and Hurrell 1994), for the period 1950-99. Contour interval is 0.005 cm/day. Red/yellow (blue) shadings indicate positive (negative) values. The NP index is a measure of the strength of the Aleutian low (area-weighted sea level pressure over the region 30ºN-65ºN, 160ºE-140ºW), with a standard deviation of 3.5 hPa in December and 4.4 hPa in January, and its sign has been reversed. Bottom: Same but for SST; contour interval is 0.01 K. The datasets employed are gridded GHCN precipitation (land-based rain-gauge station data, averaged into 5ºx5º grid boxes by using an inverse-distance weighting method) and Reynolds SST (2003). The purple line indicates the regions in which the corresponding correlation is 95% statistically significant, assuming one degree of freedom per year (r=+/- 0.27)

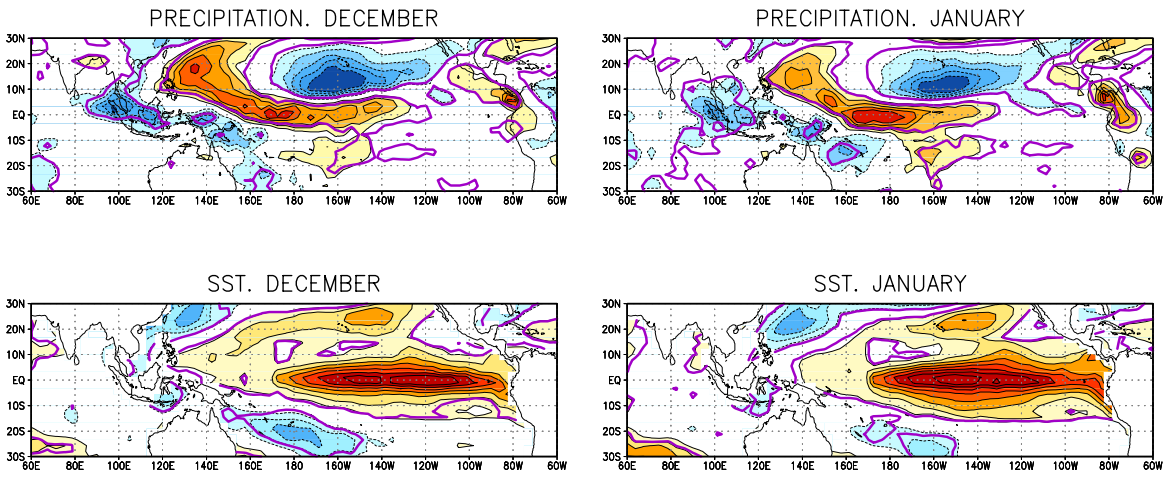

FIG. 3. Same as Fig. 2 but for the MLM-50/99 experiment (every model realization is considered an independent realization, i.e. the sampling size is 800). The model's NPI standard deviation is 4.1 hPa in December and 4.6 hPa in January. Contour interval as in Fig. 2. The purple line indicates the regions in which the corresponding correlation is 99% statistically significant, assuming one degree of freedom per year (r=+/- 0.09).

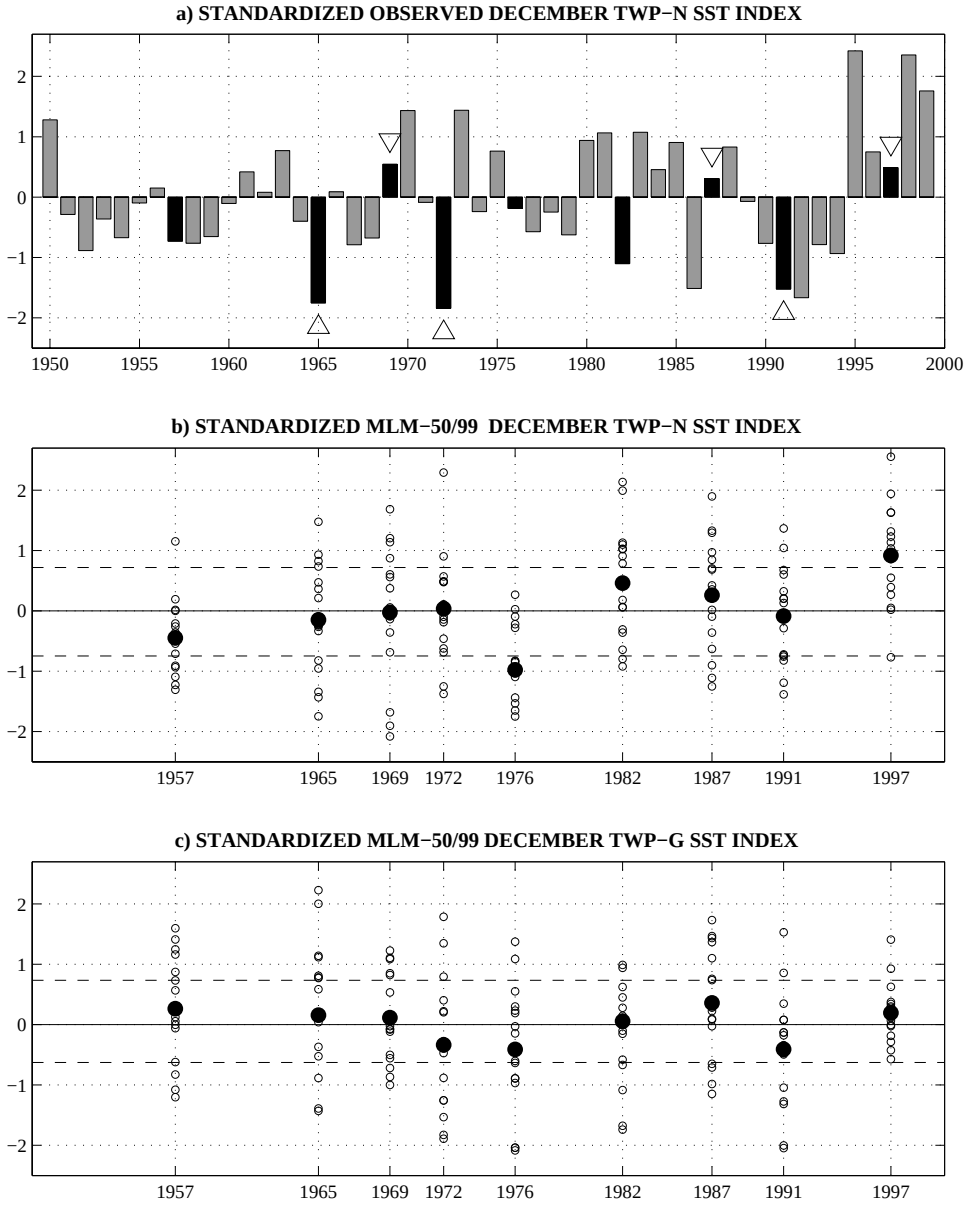

FIG. 4. Top panel: observed December TWP–N (Tropical Northwest Pacific) SST Index for the period 1950-99. The index is defined as the detrended standardized SST averaged over the region (3˚-15˚N, 135˚E-155˚E). The El Niño years are indicated with black bars. The three "LOW" and "HIGH" years, as defined by this SST index are indicated by triangles and inverted triangles, respectively. See Figs 5c or 6c for the location of the TWP–N box.

Middle panel: Simulated December TWP–N SST index for the 9 El Niño years and for each realization in the MLM-50/99 experiment. The circles denote individual realizations, the black dots denote the ensemble average for each El Niño event. The dashed lines denote the 25% and 75% percentiles and indicate which realizations enter into the UPPER and LOWER quartile composites in Fig. 5.

Bottom panel: Same but for the SST gradient index in the Tropical western Pacific (TWP–G). This index is defined as the normalized NW/SE SST gradient across New Guinea, specifically SST averaged over the TWP–N box minus SST averaged over the box (15˚S-3˚S, 115˚E-140˚E).) See Fig. 8c for the location of the boxes.

Quartile composite analysis based on TWP–N SST index (observations)

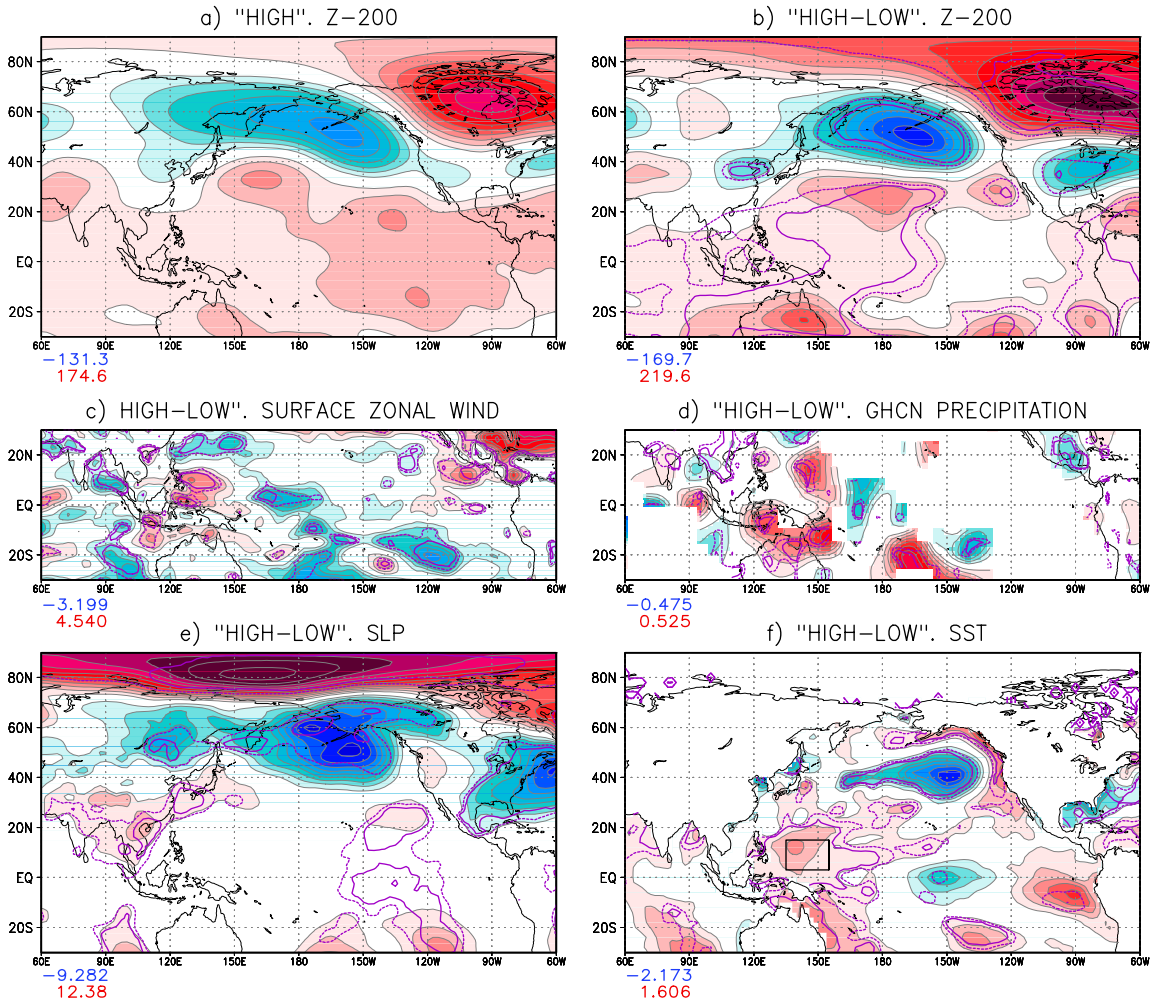

FIG. 5. Observed El Niño December anomalies stratified according to the December TWP–N SST index shown in Fig. 4a, so as to produce "HIGH" and "LOW" tercile composites. Upper tercile years: are 1969, 1987 and 1997; lower tercile years are 1965, 1972 and 1991 (cf. Fig. 4a). The area used to define the TWP–N index is indicated by a box in panel f.

a) "High" composites of 200-hPa geopotential height (Z-200). Remaining panels show the corresponding "HIGH–LOW" composite differences of b) Z-200, c) tropical surface zonal wind, d) tropical precipitation, e) SLP and f) SST. Contour/shading interval is 20 m for height, 0.067 cm/day (20 cm/month), 0.25 K for SST, 0.5 ms^{-1} for winds and 1 mb for SLP. Red (blue) shadings indicate positive (negative) values. The zero contour is omitted and shading starts at the lowest contour. The dotted (solid) purple line indicates statistical significance of the "HIGH-LOW" composite differences at the a posteriori (two-sided) 80% and 90% confidence levels. Note that wherever the sign of the difference is expected a priori (i.e. enhanced TWP–N convection, deeper North Pacific low, negative North Pacific heights), the significance levels are actually 90% and 95%.

Quartile composite analysis based on TWP–N SST index (model)

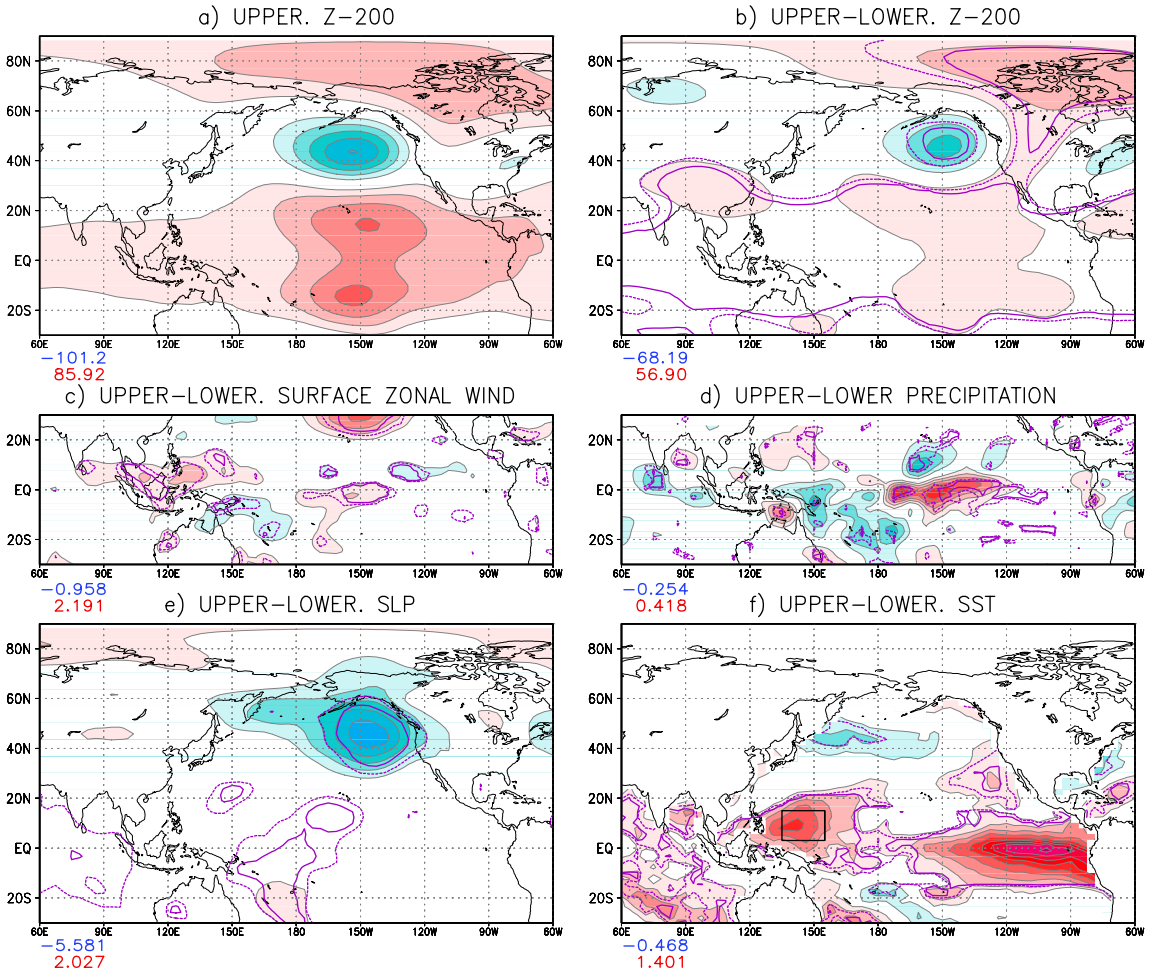

FIG. 6. Similar to Fig. 5, but for the MLM-50/99 experiment. Simulated El Niño December anomalies stratified according to the December TWP–N SST index shown in Fig. 4b, so as to produce UPPER and LOWER quartile composites (each containing 36 samples). The area used to define the TWP–N index is indicated by a box in panel f. Contour/shading interval is 20 m for height, 0.067 cm/day (20 cm/month) for precipitation, 0.15 K for SST, 0.5 ms^{-1} for winds and 1 mb for SLP. The zero contour is omitted and shading starts at the lowest contour. The dotted (solid) purple line indicates statistical significance of the "UPPER–LOWER" composite differences at the a posteriori (two-sided) 95% and 99% confidence levels. Note that wherever the sign of the difference is expected a priori (i.e. enhanced TWP–N convection, deeper North Pacific low, negative North Pacific heights), the significance levels are actually 97.5% and 99.5%. The absolute anomalies in panel (a) are computed relative to the ensemble-mean 50-year climatological mean.

Quartile composite analysis based on NPI SLP index (model)

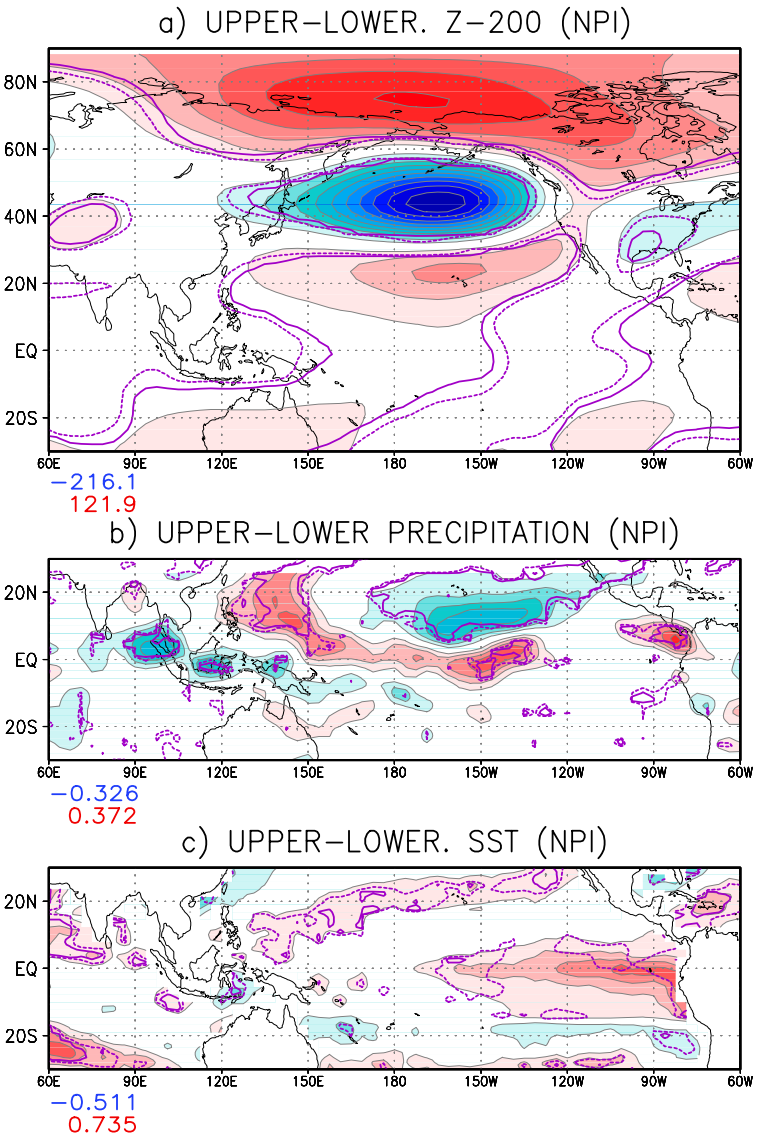

FIG. 7. As in the left panels of Figure 6, but the quartile composites are based on the North Pacific index (NPI). The sign convention is such that the UPPER quartile composite corresponds to an enhanced Aleutian low (strongly negative NPI). Contours and shading as in Fig. 6.

Quartile composite analysis based on TWP–G SST index (model)

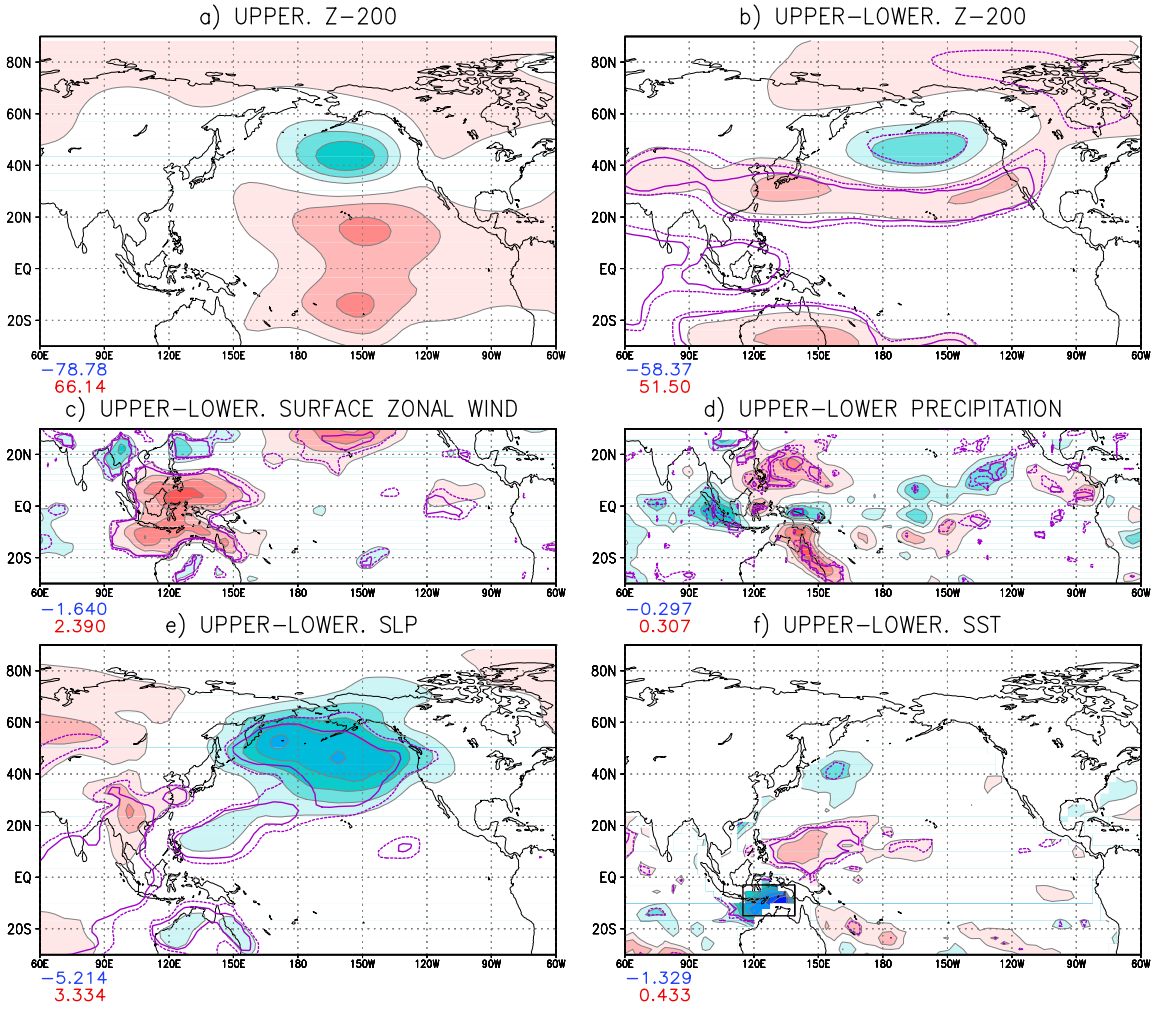

FIG. 8. As in Figure 6 but the quartile composites are based on the SST gradient index in the Tropical western Pacific, TWP–G. The areas used to define the TWP–G index are indicated by boxes in panel f. Contours and shading as in Fig. 6.

Impact of coupling in experiment TROPMLM : DECEMBER 1997

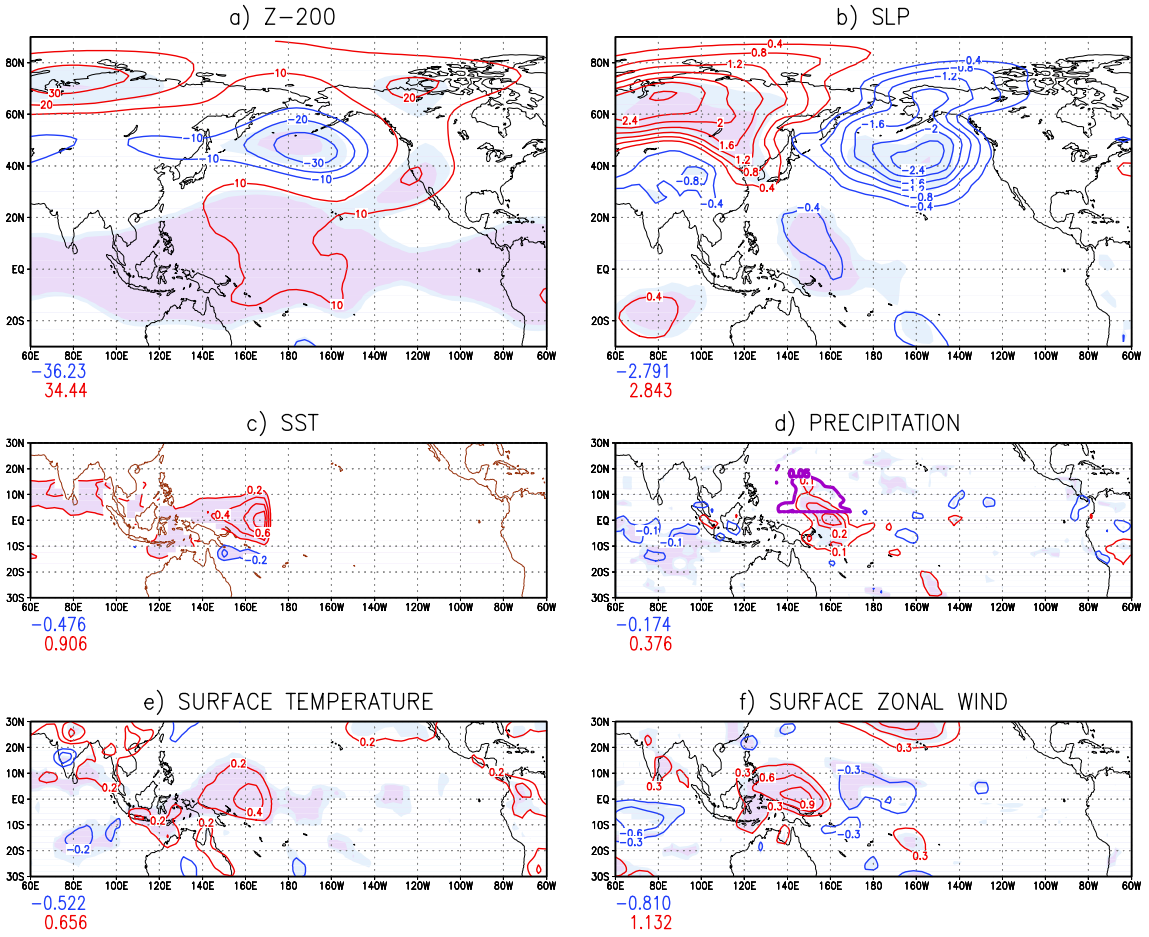

FIG. 9. December 1997 TROPMLM – CTRL anomaly differences in a) 200-hPa height, b) SLP, c) SST, d) precipitation, e) surface air temperature, and f) surface zonal wind. Contour interval is 10 m, 0.4 mb, 0.2 K, 0.1 cm day^{-1}, 0.2 K, and 0.3 ms^{-1}. The zero contour is omitted. The two grades of shading denotes statistical significance of the differences at the a posteriori (two-sided) 95% and 99% confidence levels. The purple line in panel (d) indicates the averaging region used to construct the TWP–N precipitation index, and is defined by the 0.05 cm day^{-1} precipitation contour, north of 3ºN.

Quartile composite analysis: TWP–N precipitation index (model)

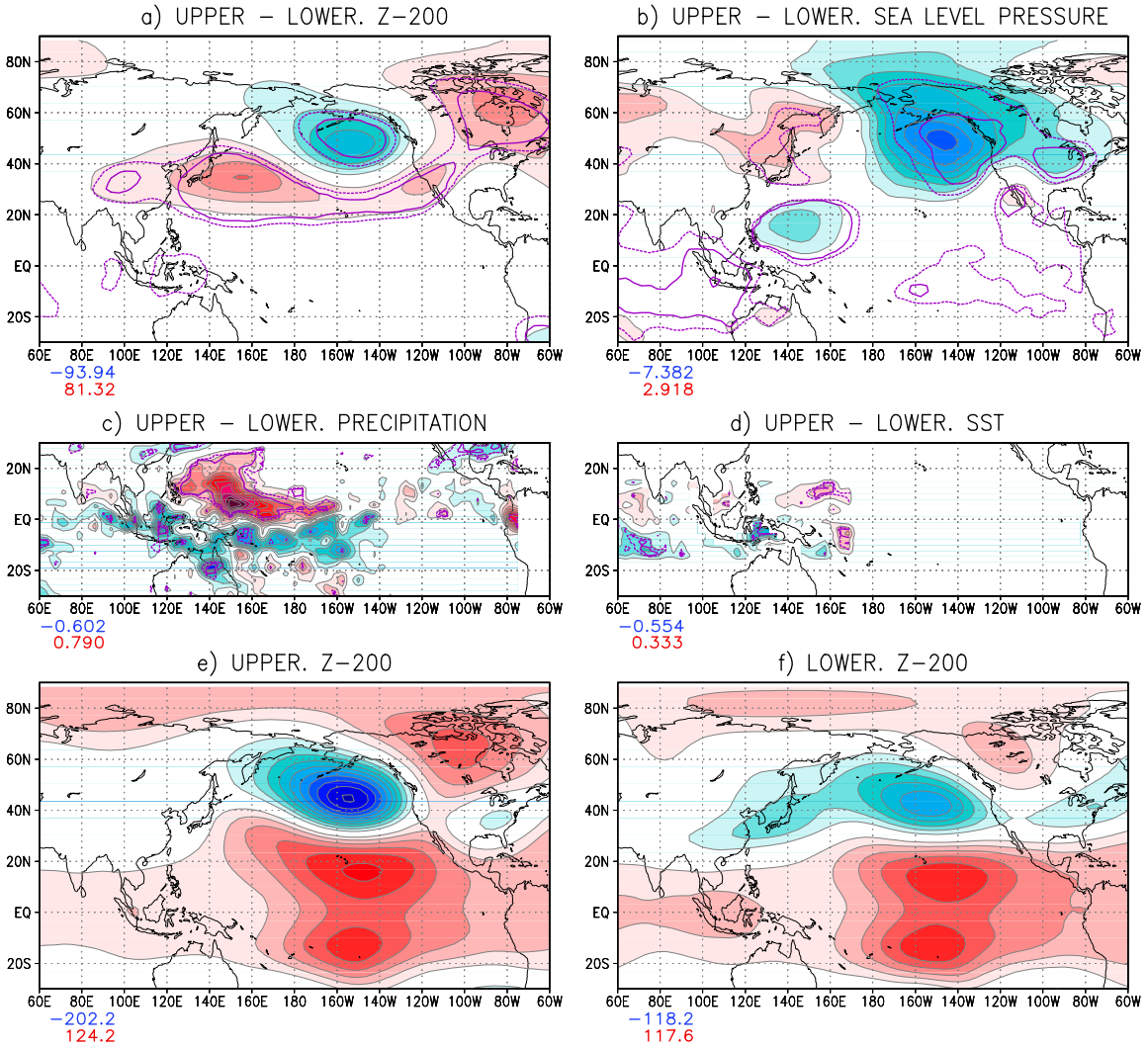

FIG. 10. UPPER–LOWER quartile composite differences, based on the TWP–N precipitation index (see purple line in Fig. 9d), for a) 200-hPa height, b) sea level pressure, c) precipitation and d) SST in December 1997 in the TROPMLM experiment. Contour/shading interval is 20 m, 1 mb, 0.0667 cmday^{-1} and 0.1 K respectively. Red (blue) shadings indicate positive (negative) values. The zero contour is omitted and shading starts at the lowest contour. The dotted (solid) purple lines indicates statistical significance (95% and 99% two-sided confidence levels). The sample size in each upper/lower composite is 25. Also shown in the bottom panels are the UPPER and LOWER quartile composites of 200-hPa height (same contour interval as in panel a).

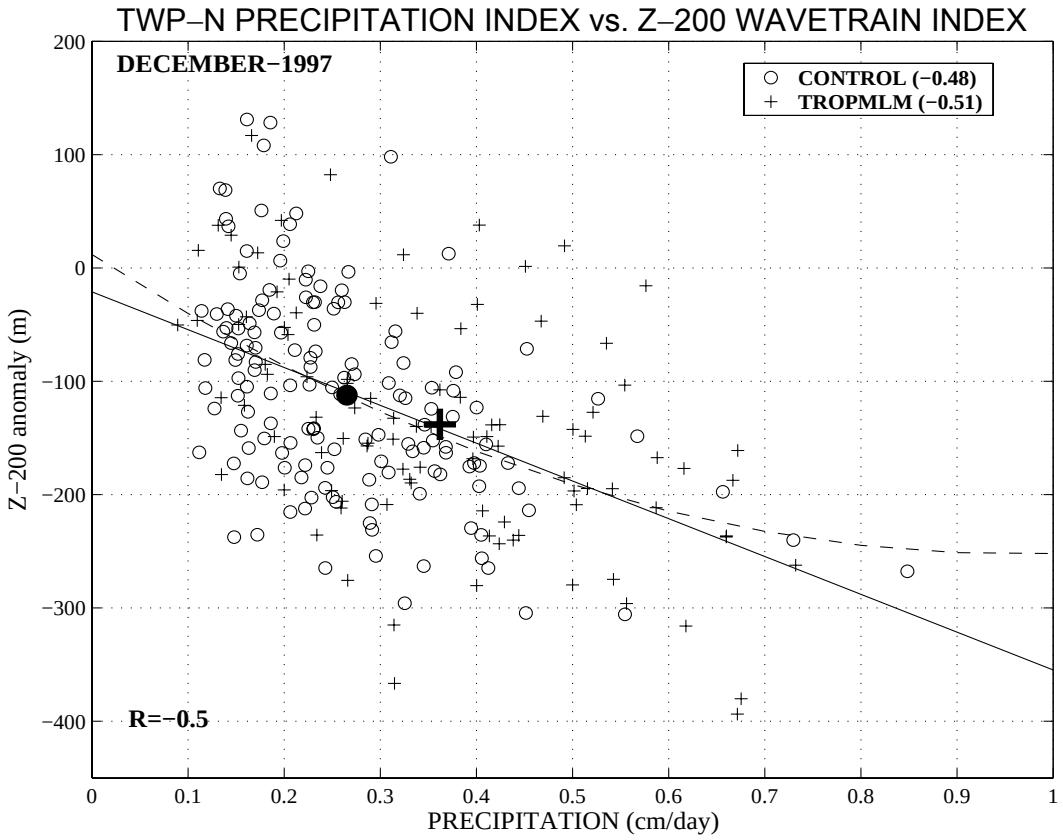

FIG. 11. Scatter plot between the December 1997 TWP−N precipitation index and the 200-hPa North Pacific wavetrain index in experiments CTRL and TROPMLM. The precipitation index is defined as the total precipitation averaged within the purple line in Fig 9d. The 200-hPa North Pacific wavetrain index is defined as the difference between the 200-hPa anomalies averaged over the northeastern Pacific and western Pacific centers of action in Fig. 10a (areas within the -60 m contour). The number in the lower left corner indicates the correlation coefficient obtained pooling all data together. The correlation for each individual experiment is indicated in the legend box. The solid (dashed) line represents a linear (quadratic) fit to the data. The thick dot and cross represent the ensemble-mean mean CTRL and TROPMLM values respectively.

IMPACT OF COUPLING ON TWP –N PRECIPITATION

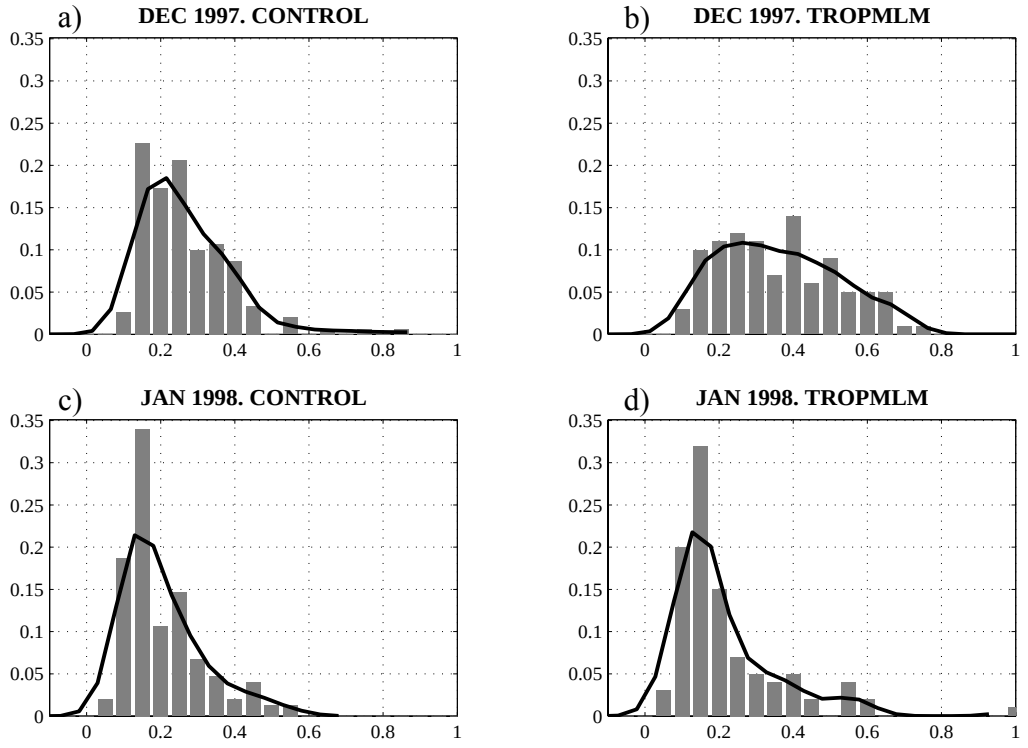

FIG. 12. Normalized histogram (bars) and probability density function (lines), estimated with a Gaussian Kernel, of monthly-mean December 1997 (top) and January 1998 (bottom) total precipitation (in cm day^{-1}) averaged over the TWP–N precipitation region, in the CTRL (left) and TROPMLM (right) experiments.

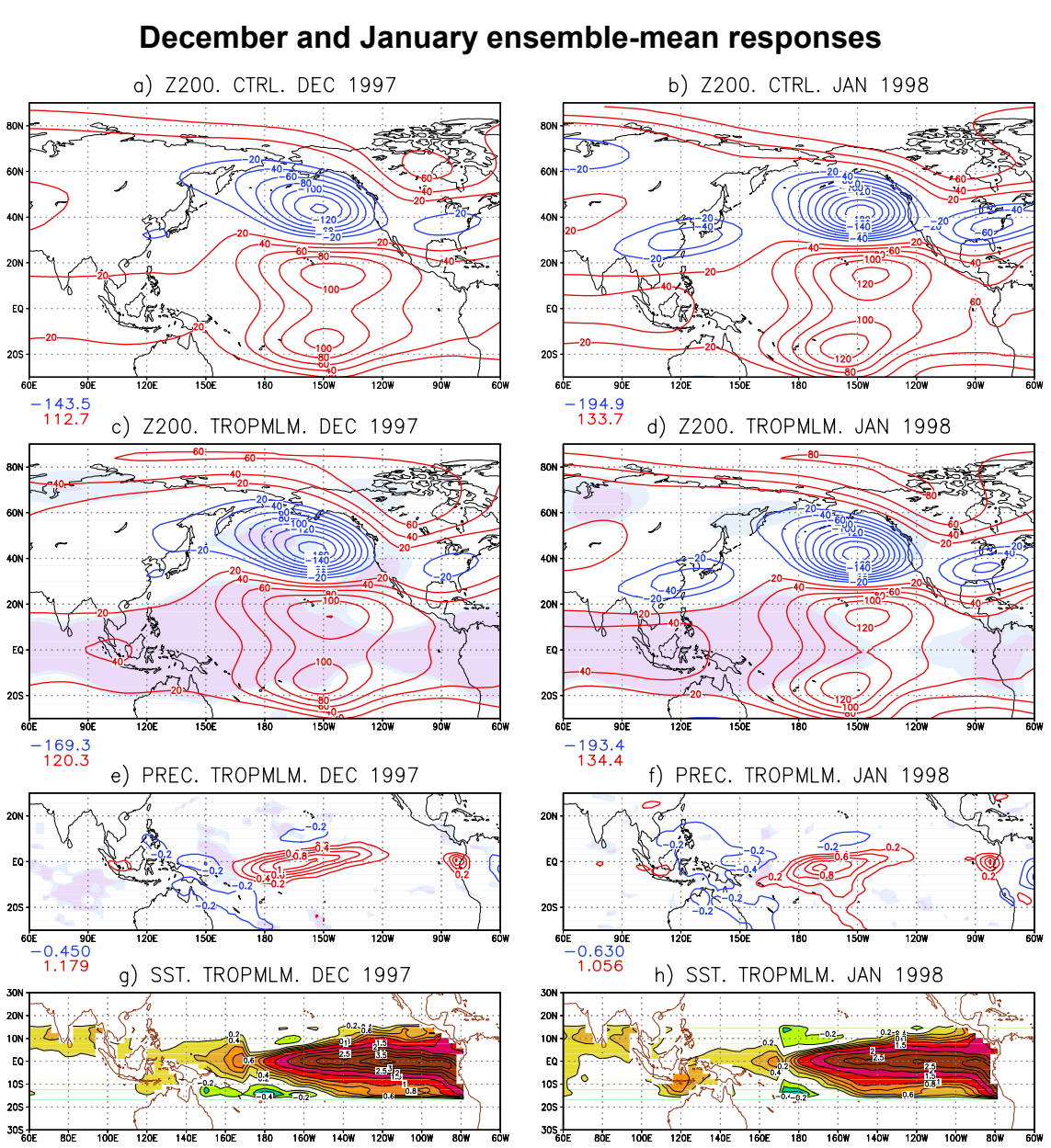

Fig. 13. The December and January ensemble-mean response to El 1997/98 Niño event in the uncoupled (CTRL) and tropically-coupled (TROPMLM) experiments. Top panels: December and January Z-200 anomalies in the CTRL experiment. Below: same but for the TROPMLM experiment. Below: same but for the precipitation anomalies. Bottom panels: same but for the SST anomalies. Anomalies are computed relative to the ensemble-mean 4-year mean in the NEUTRAL experiment. The shading in the top three rows indicates statistical significance of the TROPMLM–CTRL differences at the 95% and 99% two-sided confidence levels. Contour level is 20 m, 0.2 cm/day and 0.2 K, respectively. Note that the SST anomalies in the tropical eastern Pacific, east of 172˚E, are prescribed in both the TROPMLM and CTRL experiments.

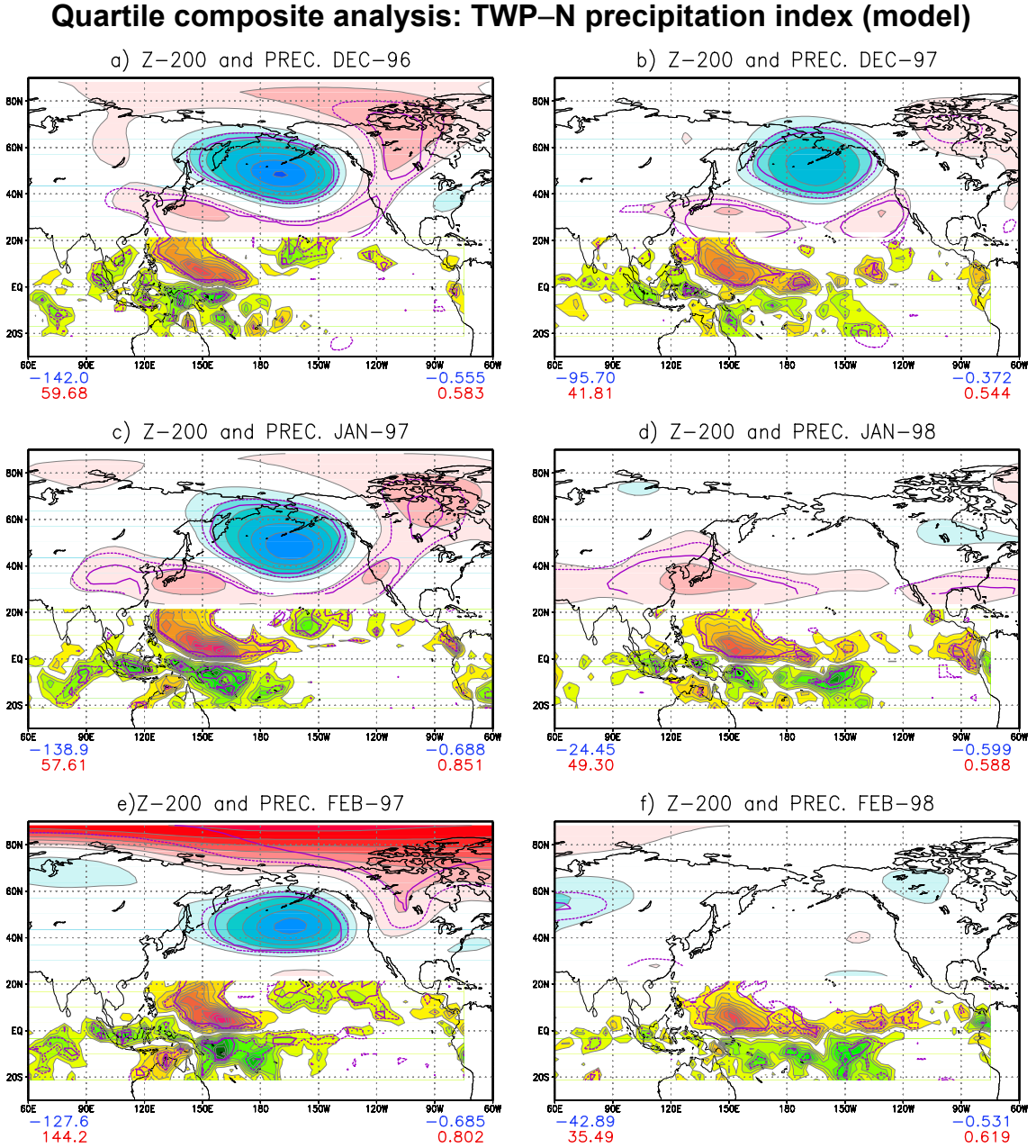

FIG. 14. CTRL experiment. UPPER–LOWER quartile composite differences of tropical precipitation (orange and green shading) and NH extratropical 200-hPa height (red and blue shading) in December, January and February, for the non-ENSO 1996/97 winter (left panel) and for the El Niño 1997/98 winter (right panel), based on the TWP–N precipitation index (see Fig. 9d). The dashed and solid purple lines indicate statistically significant differences (95% and 99% levels). Contour interval is 0.0667 cmday^{-1} and 20 m. The sample size in each upper/lower composite is 38.

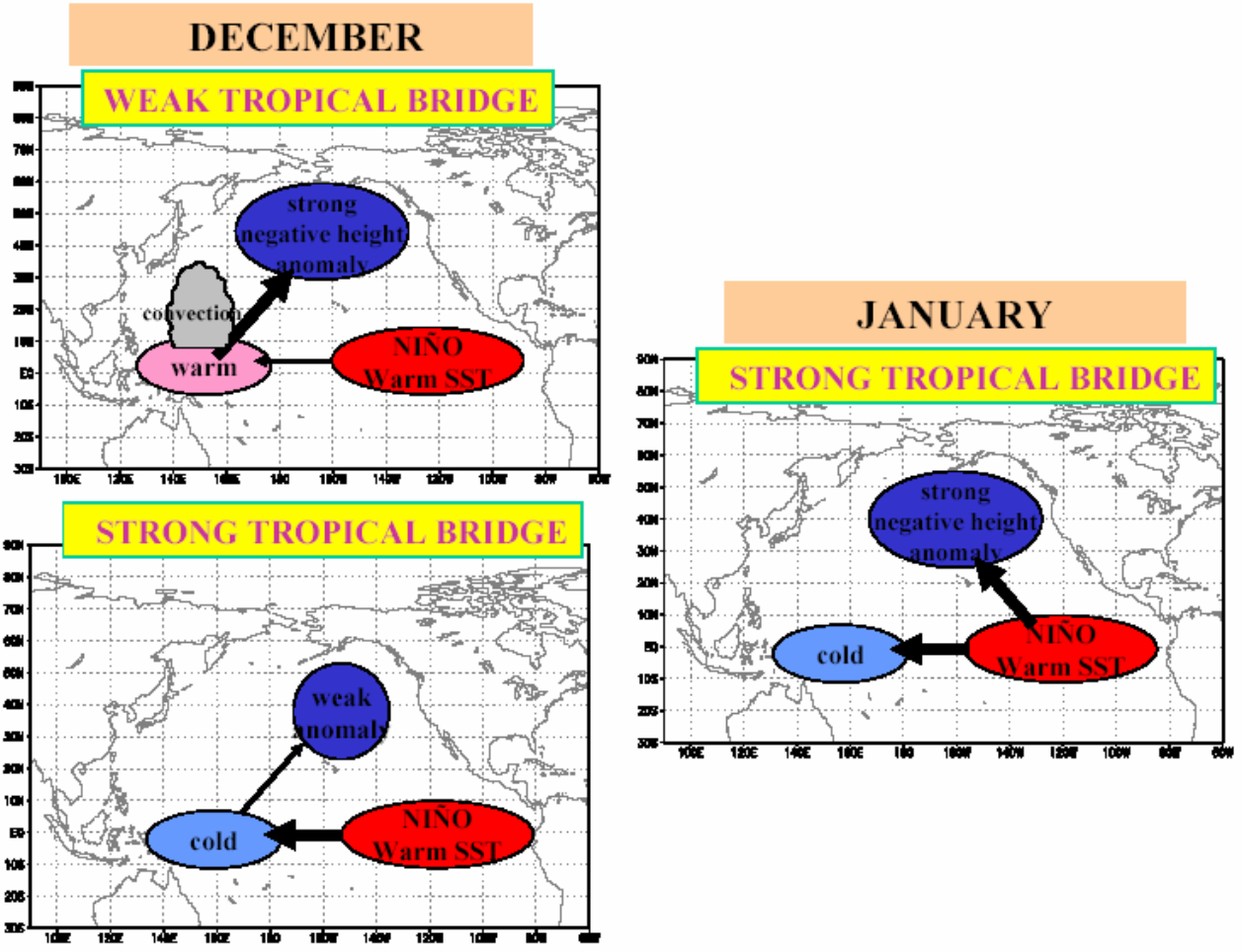

Fig. 15. Schematic of proposed hypothesis for the El Niño teleconnections. In January the tropical bridge from the TEP to the TWP is generally well established for both weak and strong El Niño events, which creates cold conditions in the TWP. More importantly, the North Pacific circulation is more sensitive to forcing from the TEP, so the El Niño teleconnection is modulated by variations in this TEP forcing. In December, however, some El Niño events are characterized by a weakened tropical bridge and warm conditions in the TWP, which supports the development of local convection. Because of the enhanced sensitivity of the North Pacific circulation to forcing from the TWP in late fall, the extratropical El Niño response will be much stronger.

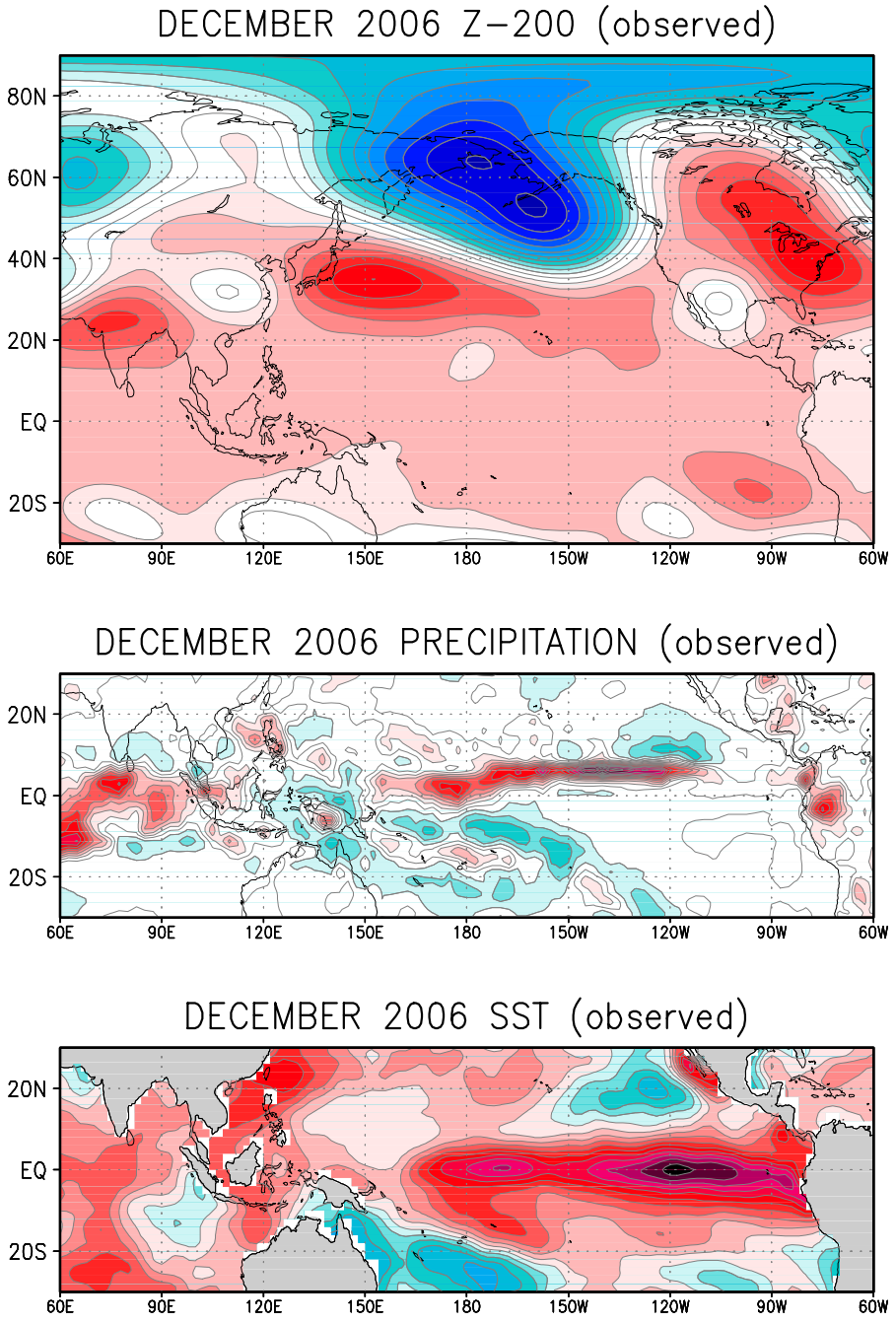

Fig. 16. Observed NCEP Z-200, GPCP precipitation and NOAA SST December anomalies for the 2006/07 El Niño event. The anomalies are computed relative to the 1950-99 climatology (for consistency with the rest of the paper), except for the GPCP data (for which the climatology can only be computed for the period 1979-19). Contour/shading interval is 20 m, 0.15 cm/day and 0.2 K, respectively. Red (blue) shadings indicate positive (negative) values. The zero contour is omitted and shading starts at the lowest contour (except in the lower panel).

Table I: Description of all experiments referred to in this study. The experiments extensively analyzed are marked in boldface. The other experiments are either only mentioned in passing (CTRL−50/99, MLM) or are required to define a neutral basic state relative to which to compute monthly-mean anomalies (NEUTRAL). "Climatological" refers to the corresponding MLM run ensemble-mean long-term mean SSTs. These are the yearly-repeating SST prescribed in the uncoupled regions outside the tropical eastern Pacific (see text).

Experiment name	***Period***	***Number of simulations***	***SST field in tropical eastern Pacific***	***Coupling configuration***
CTRL-1950/99	1950-99	8	observed	No coupling
MLM-1950/99	**1950-99**	**16**	**observed**	**coupling in entire ice-free oceanic domain**
NEUTRAL	1996-99	150	"climatological"	no coupling
CTRL	**1996-99**	**150**	**observed**	**no coupling**
TROPMLM	**1996-99**	**100**	**observed**	**coupling in tropical Indian and western Pacific oceans**
MLM	1996-99	150	observed	coupling in entire ice-free oceanic domain